Pex24 and Pex32 are required to tether peroxisomes to the ER for organelle biogenesis, positioning and segregation

Fei Wu[1,4], Rinse de Boer[1,4], Arjen M. Krikken[1], Arman Akşit[1], Nicola Bordin[2,3], Damien P. Devos[2] and Ida J. van der Klei[1*]

[1]Molecular Cell Biology, Groningen Biomolecular Sciences and Biotechnology Institute, University of Groningen, the Netherlands

[2]Centro Andaluz de Biología del Desarrollo, CSIC, Universidad Pablo de Olavide, Carretera de Utrera, Km.1, Seville 41013, Spain

[3]Current address: Structural and Molecular Biology, University College London WC1E 6BT, UK

[4]These authors contributed equally to the work.

*Corresponding author: i.j.van.der.klei@rug.nl, ORCID ID 0000-0001-7165-9679, P.O. Box 11103, 9700CC, Groningen, The Netherlands

Running title: Pex23 family proteins

Keywords: Peroxisome, Pex24, Pex32, endoplasmic reticulum, membrane contact, yeast

Summary statement

The absence of Pex24 or Pex32, two *Hansenula polymorpha* ER proteins, disturbs peroxisome-ER contact sites and leads to multiple peroxisomal defects, which can be restored by an artificial tether protein.

Abstract

The yeast *Hansenula polymorpha* contains four members of the Pex23 family of peroxins, which characteristically contain a DysF domain. Here we show that all four *H. polymorpha* Pex23 family proteins localize to the ER. Pex24 and Pex32, but not Pex23 and Pex29, predominantly accumulate at peroxisome-ER contacts. Upon deletion of *PEX24* or *PEX32* - and to a much lesser extent of *PEX23* or *PEX29* - peroxisome-ER contacts are lost, concomitant with defects in peroxisomal matrix protein import, membrane growth, organelle proliferation, positioning and segregation. These defects are suppressed by the introduction of an artificial peroxisome-ER tether, indicating that Pex24 and Pex32 contribute to tethering peroxisomes to the ER. Accumulation of Pex32 at these contact sites is lost in cells lacking the peroxisomal membrane protein Pex11 in conjunction with disruption of the contacts. This indicates that Pex11 contributes to Pex32-dependent peroxisome-ER contact formation. The absence of Pex32 has no major effect on pre-peroxisomal vesicles that occur in *pex3 atg1* cells.

Introduction

Peroxins are defined as proteins that play a role in peroxisome biogenesis, including peroxisomal matrix protein import, membrane biogenesis and organelle proliferation (Distel et al., 1996). Most peroxins are peroxisomal or cytosolic proteins, which transiently are recruited to the organelle. Recent studies in bakers' yeast showed that a family of peroxins, called the Pex23 protein family (Kiel et al., 2006), localize to the endoplasmic reticulum (ER) (David et al., 2013; Joshi et al., 2016; Mast et al., 2016). The function of these peroxins is still poorly understood and is the subject of this study.

Proteins of the Pex23 family are characterized by a DysF domain. The DysF domain was first identified in human dysferlin. Dysferlin is important for fusion of vesicles with the sarcolemma at the site of muscle injury (Bansal and Campbell, 2004; North et al., 2011; Bansal et al., 2003). Human dysferlin contains multiple C2 domains, which play a direct role in the above membrane repair process, however the function of the DysF domain in dysferlin is still obscure.

Yarrowia lipolytica Pex23 was the first DysF domain containing peroxin that was identified (Brown et al., 2000). The number of Pex23 family members varies in different yeast species and their nomenclature is confusing (see Fig. 1A). *Hansenula polymorpha* and *Pichia pastoris* contain four members, but *Saccharomyces cerevisiae* has five and *Y. lipolytica* has only three. Mutants lacking one of these peroxins show diverse peroxisomal phenotypes ranging from a partial peroxisomal matrix protein import defect to enhanced or decreased peroxisome numbers (Brown et al., 2000; Tam and Rachubinski, 2002; Vizeacoumar et al., 2003, 2004; Yan et al., 2008).

Initially, Pex23 family proteins were thought to localize to peroxisomes (Brown et al., 2000; Tam and Rachubinski, 2002; Vizeacoumar et al., 2003, 2004; Yan et al., 2008). However, later studies indicated that *S. cerevisiae* Pex23 family proteins are ER proteins and form complexes with the ER resident reticulons Rtn1/Rtn2 and Yop1 (David et al., 2013; Mast et al., 2016). *S. cerevisiae* Pex30 and its paralog Pex31 have been implicated in the formation of peroxisome-ER contact sites, where they regulate *de novo* peroxisome formation from the ER (David et al., 2013; Joshi et al., 2016; Mast et al., 2016; Wang et al., 2018). *S. cerevisiae* Inp1 also has been implicated in the formation of peroxisome-ER contacts, but serves a different function, namely in peroxisome retention during yeast budding (Knoblach et al., 2013).

ScPex30 and ScPex31 contain a reticulon-like domain and have membrane shaping properties (Joshi et al., 2016). ER-regions where Pex30 accumulates are important for the regulation of pre-peroxisomal vesicle (PPV) formation, but also play a role in lipid droplet biogenesis (Joshi et al., 2018; Wang et al., 2018; Lv et al., 2019).

So far, *S. cerevisiae* Pex29, Pex30 and Pex31 have been extensively studied. However, our knowledge on other members of the *S. cerevisiae* Pex23 protein family as well as on these proteins from other yeast species is still relatively scarce.

Here, we studied all four Pex23 family members of the yeast *H. polymorpha*. Our results indicate that these proteins localize to the ER and accumulate at membrane contact sites, including peroxisome-ER contacts and nucleus vacuole junctions (NVJs). Pex24 and Pex32, but not Pex23 and Pex29, predominantly localize to peroxisome-ER contact sites. Moreover, deletion of *PEX24* or *PEX32* - but not of *PEX23* or *PEX29* - results in major aberrations in peroxisome biology, including defects in peroxisomal matrix protein import and membrane growth, organelle proliferation, positioning and segregation. These defects are accompanied by the disruption of close associations between the peroxisomal and ER membranes, indicating that these proteins are crucial for peroxisome-ER contact site formation. Introduction of an artificial peroxisome-ER tether suppresses the peroxisomal phenotypes, indicating that Pex24 and Pex32 contribute to tethering of peroxisomes to the ER.

Further studies on the function of Pex32 indicated that the accumulation of this protein at peroxisome-ER contacts is lost in cells lacking the peroxisomal membrane protein Pex11. Moreover, in *pex11* cells peroxisome-ER contacts are defective like in *pex32* cells. These results are consistent with the view that Pex11 is also important for peroxisome-ER associations. Deletion of *PEX32* in *pex3 atg1* cells did not result in a change in the abundance or morphology of PPVs, suggesting that Pex32 is not involved in the regulation of PPV formation.

RESULTS

Protein sequence and structure prediction

Construction of a phylogenetic tree of Pex23 family members of four different yeast species indicated that two subfamilies (the Pex23 and Pex24 subfamilies) can be distinguished (Fig. 1A). All *H. polymorpha* members contain a DysF domain at the C-terminus. HpPex32 is much shorter than the others, which is mostly due to the lack of an unstructured fragment at the amino-terminus of this protein (Fig 1B).

HpPex23 ends with a KKKE stretch of residues, similar to the KKXX found in *S. cerevisiae* Pex30 (David et al., 2013). *H. polymorpha* Pex24 ends with KKR. These C-termini may represent di-lysine motifs, which are recognized by coatomer subunits and important for retrograde transport to the ER (Ma and Goldberg, 2013). The C-termini of HpPex29 and HpPex32 do not contain di-lysine motifs.

Secondary structure prediction indicated that all four sequences contain between two to four transmembrane helices and a C-terminal domain dominated by beta-sheets (Fig. 1B). It has been previously argued that a reticulon-like domain was observed in this family of proteins, particularly in ScPex30 and ScPex31 (Joshi et al., 2016). Indeed, a similar hit can be found on HpPex23 using HHpred on the Pfam-A database. This detection extends from residue 100 to 233 of HpPex23. However, this detection has an E-value of 2 with a probability of 92.38, making it a borderline detection. Similar borderline hits are detected in HpPex24, HpPex29 and HpPex32. A Trp residue is also present at the N terminus of this potential domain and aligns with the classical Trp conserved residue of other Pex reticulon-like domains.

All *H. polymorpha* Pex23 family members localize to the ER

The localization of the four *H. polymorpha* Pex23 family proteins was determined by fluorescence microscopy (FM) using strains producing C-terminal GFP tagged proteins under control of their endogenous promoters (Fig. 2A,B). Functional peroxisomes are essential for growth of *H. polymorpha* on methanol. All four strains grew similar as the wild-type (WT) control on media containing methanol, indicating that tagging with GFP at the extreme C-terminus does not affect the function of Pex23 family proteins in peroxisome biology (Supplementary Table 1).

Protein localizations were performed using cells that were grown in media containing glucose (peroxisome repressing conditions). At these conditions the cells generally contain a single small peroxisome that is associated to the ER (Wu et al., 2018). As shown in Fig. 2B, all four proteins co-localized with the ER marker BiP-mCherry-HDEL, predominantly at the cortical ER. Frequently, a patch of Pex23-GFP was observed at the nuclear envelope as well (Fig. 2A,B). In Pex24-GFP or Pex32-GFP producing strains generally one fluorescent spot was detected per cell, which invariably localized close to the single peroxisome marked with Pex14-mKate2. More fluorescent spots were present in cells of Pex23-GFP and Pex29-GFP producing strains and one of them invariably was present in the vicinity of the Pex14-mKate2 spot (Fig. 2A).

Upon overproduction, all four HpPex23 proteins showed a typical cortical ER/nuclear envelope pattern, supporting that they represent genuine ER proteins. FM analysis revealed that the overproduced proteins were not evenly distributed over the ER, but present in spots and patches. In all strains one cortical patch localized in the vicinity of the peroxisome (here marked with DsRed-SKL) (Fig. 2C). Relatively large patches of GFP fluorescence were frequently observed at the nuclear envelope in cells overproducing Pex24-GFP. Co-localization studies with the nucleus-vacuole junction (NVJ) protein Vac8 indicated that these patches represent NVJs (Fig. 2D). Pex23-GFP also accumulated at NVJs when produced under control of its own promoter.

Western blot analysis showed that the levels of all four GFP fusion proteins were very low when produced under control of their endogenous promoters. In fact, Pex24-GFP and Pex32-GFP were below the limit of detection, whereas faint bands were detected on blots of Pex23-GFP and Pex29-GFP producing cells. Upon overproduction all four GFP-fusion proteins were readily detected (Fig. 2E).

Our data support observations in *S. cerevisiae*, where Pex23 family proteins localize to the ER, including at regions where peroxisomes and ER are in close vicinity (David et al., 2013; Mast et al., 2016). The presence of a portion of HpPex23 and overproduced HpPex24 at NVJs suggest that Pex23 family proteins are also components of other membrane contacts.

The absence of Pex24 and Pex32 affect peroxisome biogenesis and abundance

To study the role of the Pex23 family proteins we constructed four *H. polymorpha* deletion strains, *pex23*, *pex24*, *pex29* and *pex32*. First, we analyzed whether Pex23 family proteins are important for peroxisomal matrix protein import using glucose-grown cells producing the matrix marker GFP-SKL and wide field fluorescence microscopy (FM). GFP-SKL mislocalized to the cytosol in a portion of the *pex32* cells (Fig. 3A), while cytosolic fluorescence was occasionally observed in *pex23* and *pex24* cells, but never in *pex29* cells. In *pex32* cultures, typically three types of cells could be discriminated, namely i) cells with a GFP spot without cytosolic fluorescence, ii) cells with a GFP spot in conjunction with cytosolic GFP and iii) cells with only cytosolic GFP. This indicates that although matrix protein import is strongly compromised in some of the cells, Pex32 is not essential for the assembly of a functional importomer.

Next, we quantified the number of GFP containing spots by confocal laser scanning microscopy (CLSM) and a custom-made plugin for ImageJ (Thomas et al., 2015). In these images cytosolic fluorescence was not detected in any of the strains due to the lower sensitivity of CLSM relative to wide field FM. The average number of GFP spots per cell was similar in WT and *pex29* cells but reduced in the other three deletion strains. The strongest reduction was observed in *pex24* and *pex32* cells (Fig. 3B). Frequency distribution graphs show that these reductions are accompanied by an increase in the percentage of cells lacking a GFP spot (Fig. 3B). These results indicate that Pex24 and Pex32 are important for normal peroxisome abundance.

Finally, we analyzed the strains at peroxisome inducing growth conditions (methanol). Mislocalization of peroxisomal matrix enzymes affects methylotrophic growth (van der Klei et al., 2006). We therefore routinely grow peroxisome-deficient mutants on a mixture of glycerol and methanol (Knoops et al., 2014). At these conditions, cells grow on glycerol (which does not require peroxisome function), while methanol is used as additional carbon and energy source, depending on the severity of the peroxisome function defect. Growth experiments using glycerol/methanol media revealed the strongest growth defects for the *pex32* and *pex24* strains. Cells of the *pex23* strain showed only a minor reduction in growth, whereas *pex29* cells grew like WT controls (Fig. 3D). These data indicate that the function of peroxisomes is strongly compromised in the absence of Pex24 and Pex32, but not in cells lacking Pex29.

Quantification of structures marked with the peroxisomal membrane marker Pmp47-GFP indicated that relative to WT controls also at these growth conditions peroxisome abundance was reduced, especially in *pex24* and *pex32* cells (Fig. 3C). Moreover, CLSM revealed that *pex23*, *pex24* and *pex32* cells frequently contained a peroxisome of enhanced size (Fig. 3C).

In conclusion, *pex24* and *pex32* cells showed the most severe peroxisomal phenotypes, while *pex29* cells were like WT and *pex23* cells had minor peroxisomal defects.

The absence of Pex23 family proteins disrupts peroxisome-ER contacts

In *S. cerevisiae*, Pex23 family proteins and Inp1 play a role in the formation of peroxisome-ER contacts (David et al., 2013; Knoblach et al., 2013; Mast et al., 2016). By measuring the distance between peroxisomal and ER membranes in electron micrographs, we analyzed the role of *H. polymorpha* Pex23 proteins in the formation of peroxisome-ER contacts (Fig. 4). At membrane contact sites two membranes are usually separated by a distance smaller than 30 nm. As shown in Fig. 4A, in WT controls the distance between both membranes was generally less than 10 nm for approximately 80 % of the peroxisomal profiles analyzed, while the distance was larger than 30 nm in less than 10 % of the profiles analyzed (Fig. 4A). In cells of the *pex23* and *pex29* strains for only 40 % of the organellar profiles a distance of less than 10 nm was measured, whereas this percentage further dropped in *pex24* and *pex32* cells to 10 - 20 % (Fig. 4A,B). These changes were not related to a decrease in total cortical ER, which instead slightly increased (Fig. 4D). Deletion of *INP1* had no effect on the distance at peroxisome-ER contact sites (Fig. 4C), in line with our recent observation that *H. polymorpha* Inp1 associates peroxisomes to the plasma membrane (Wu, 2020). Based on these observations we conclude that Pex24 and Pex32 - and to a lesser extent Pex29 and Pex23, but not Inp1 - play crucial roles in the formation of tight membrane contacts between peroxisome and ER membranes.

In glucose-grown WT cells, the single peroxisome is invariably localized at the cell cortex. FM analysis of the position of peroxisomes demonstrated that peroxisomes remained close to the cell cortex upon deletion of either *PEX32* or *INP1*. However, in a *pex32 inp1* double mutant peroxisomes were more frequently observed in the central part of the cells, indicating that Pex32 and Inp1 together contribute to the cortical association of peroxisomes (Fig. 4E).

In budding WT cells at least one peroxisome is retained in the mother cells, whereas another one is transported to the nascent bud. Quantification of peroxisomes in mother cells and buds indicated that the organelles normally segregated over mother cells and buds of the *pex29* strain like in WT controls. Cultures of *pex23*, *pex24* and *pex32* cells, however, showed aberrant peroxisome segregation patterns. In *pex24* cultures a large fraction of the budding cells contained peroxisomes solely in the buds, indicative for a defect in retention of peroxisomes in mother cells (Fig. 4F). A similar, but stronger retention defect was observed in *inp1* control cells, known to be defective in peroxisome retention (Fig. 4F).

Our data show that close associations between peroxisomes and the ER require Pex23 family proteins, of which Pex24 and Pex32 are paramount. Inp1 is not crucial for the formation of these associations. Our data furthermore show that the associations contribute to peroxisome positioning at the cell cortex and proper peroxisome segregation in budding cells.

An artificial peroxisome-ER tether suppresses the peroxisomal phenotypes

To study whether the effect of the absence of Pex24 and Pex32 on peroxisome biology is due to the loss of peroxisome-ER contacts, we introduced an artificial tether in an attempt to re-associate both organelles. This approach is based on studies in *S. cerevisiae*, in which the absence of proteins of the ER-Mitochondria Encounter Structure (ERMES) is partially complemented by artificially anchoring mitochondria to the ER (Kornmann et al., 2009). To this end we constructed an artificial tether protein consisting of full length Pex14 and the tail anchor of the ER protein Ubc6, separated by two heme-agglutinin tags (HA). This construct (P_{ADH1}Pex14-HA-HA-Ubc6^{TA}), termed ERPER, was introduced in WT and the four deletion strains (Fig. 5A). Electron microscopy (EM) showed that introduction of ERPER resulted in regions of close opposition (< 10 nm) between the ER/nuclear envelope and the peroxisomal membranes (Fig. 5B,C). Immuno-EM using anti-HA antibodies confirmed the presence of ERPER tether protein at these regions (Fig. 5B). EM also showed that in all strains producing ERPER multiple peroxisomes were present as in WT controls producing ERPER upon growth on a mixture of methanol and glycerol (Fig. 5C), which was confirmed by FM (Fig. 5D). Also, in *pex32* cells with the ERPER and producing GFP-SKL, cytosolic fluorescence was not detectable (Fig. 5D), indicating that the matrix protein import defect was suppressed by the ERPER. Peroxisome quantification showed that peroxisome numbers in *pex24* and *pex32* cells containing ERPER were similar as in WT control cells producing ERPER (Fig. 5E; compare with Fig. 3C).

Introduction of ERPER did not affect growth of WT while it partially suppressed the growth defects that were observed for the *pex24* and *pex32* deletion strains on glycerol/methanol media (Fig. 5F), confirming that the tether restored peroxisome matrix protein import and function. As expected, the tether did not affect growth of *pex29* cells on methanol (Fig. S1B). Also, the minor growth defect of *pex23* was not suppressed by ERPER, suggesting that this defect is not caused by altered peroxisome-ER contacts (Fig. S1C).

Introduction of a control construct containing P_{ADH1}Pex14, which does not cause tethering of peroxisomes to the ER, did not alter peroxisome biogenesis or function in WT cells (Fig. S1A). Only introduction of ERPER (P_{ADH1}Pex14-HA-HA-Ubc6^{TA}), but not Pex14++ (P_{ADH1}Pex14), suppressed the growth defect of *pex32* cells on glycerol/methanol, confirming that artificial tethering and not solely the enhanced Pex14 levels are responsible for suppression of the phenotype (Fig. S1D).

From this we conclude that the severe peroxisome defects in *pex24* and *pex32* cells are related to a loss in tight peroxisome-ER contacts.

Pex24 and Pex32 are important for peroxisomal membrane growth

Membrane contacts of cell organelles with the ER have been implicated in lipid transfer. To test whether the Pex24/Pex32 dependent peroxisome-ER contacts are important for expansion of peroxisomal membranes, we compared the average peroxisomal membrane surface per cell in the four deletion strains relative to the WT control. The plug-in for the analysis of CLSM images allows quantifying the average diameter of peroxisomes by fitting spheres in data obtained from the green channel of combined z-slices of glycerol/methanol grown, PMP47-GFP producing cells (Thomas et al., 2015). From these data we estimated the average peroxisomal membrane surface per cell. As shown in Fig. 5G, these values were reduced in *pex24* and *pex32* cells relative to *pex23, pex29* and WT cells. Because we are aware of the drawbacks of analyzing organelle sizes by FM (the limited resolution of FM may cause an overestimation of the diameter of very small organelles that are more abundant in WT cells), we also quantified the average length of peroxisomal membranes in cell sections using EM (Fig. 5H). This analysis confirmed that in especially in *pex32* cells, but also in *pex24* cells, the peroxisomal membrane surface is reduced.

Similar analyses of the *pex24* and *pex32* strains containing ERPER showed that the average peroxisome membrane surface area per cell increased again (Fig. 5G,H), suggesting that the Pex24- and Pex32-dependent contacts may contribute to lipid supply and hence peroxisomal membrane expansion.

Pex23, Pex24 and Pex29 are not functionally redundant with Pex32

Because *pex32* cells showed the strongest peroxisome phenotype, we confined our further studies to Pex32.

First, we analyzed whether the phenotype of *pex32* cells could be suppressed by overproduction of any of the other members of the Pex23 protein family. To this purpose the corresponding genes were placed under control of the strong amine inducible amine oxidase promoter (P_{AMO}). Quantitative analysis of FM images of glucose/methylamine-grown cells indicated that upon overexpression of *PEX32* in *pex32* cells peroxisome numbers increased. This was not the case upon overexpression of *PEX23*, *PEX24* or *PEX29* (Fig. 6A). Similarly, overexpression of *PEX32,* but not of *PEX23, PEX24* or *PEX29* almost completely restored the defect of *pex32* cells to grow on methanol (Fig. 6B). These data show that *PEX23*, *PEX24* and *PEX29* are not functionally redundant with *PEX32*.

Pex32-GFP concentrates at peroxisome-ER membrane contact sites

Next, we performed correlative light and electron microscopy (CLEM) to analyze Pex32-GFP localization at high resolution. In order to obtain sufficient fluorescence signal, Pex32-GFP was slightly overexpressed by placing the gene under control of the P_{AMO} and inducing this promoter for a short period. At these conditions generally only a single fluorescent spot was detected per cell. EM analysis revealed that the fluorescent spot characteristically localizes at the region where the ER and peroxisomal membrane were closely associated (Fig. 6C). In total four tomograms were analyzed and in all the Pex32-GFP dependent fluorescent spot was present at the peroxisome-ER contact.

Pex11 is required for the formation of peroxisome-ER contact sites and the concentration of Pex32-GFP at these sites

Next, we examined whether the peroxisome-ER association is required for concentrating Pex32. To address this, we localized Pex32-GFP in a *pex3 atg1* double deletion strain, which lacks normal peroxisomes but contains PPVs (Knoops et al., 2014). In these cells Pex32-GFP accumulation in a spot was lost. Instead, multiple fainter Pex32-GFP spots were observed (Fig. 6D). In a *pex5 atg1* control strain generally one or a few Pex32-GFP spots were present, like observed in WT cells. In *pex5 atg1* cells small peroxisomes occur that are defective in PTS1 protein import but harbor the complete set of PMPs. Because PPVs in *pex3 atg1* cells and peroxisomes in *pex5 atg1* cells differ in PMP composition, we argued that those PMPs that are absent in PPVs may contribute to the accumulation of Pex32-GFP in spots. One of these PMPs is Pex11 (Knoops et al., 2014). We therefore also tested the effect on Pex32-GFP spots in cells lacking Pex11. FM indicated that in *pex11* cells, but not in *pex25* controls, the bright Pex32-GFP spots were lost (Fig. 6D). Pex25 is also a PMP and belongs to the same protein family as Pex11. Western blot analysis showed that Pex32-GFP levels in these mutants are similar to WT controls, indicating that the absence of the clear Pex32-GFP spots was not due to reduced protein levels (Fig. S2). These data suggest that Pex11, but not Pex25, is specifically required for the accumulation of Pex32-GFP at peroxisome-ER contact sites.

H. polymorpha pex11 cells have several features in common with *pex32* cells. These cells show reduced growth on methanol, contain less, but larger peroxisomes and show a peroxisome segregation defect (Krikken et al., 2009). This led us to examine whether *pex11* cells are also defective in peroxisome-ER contacts. Indeed, EM analysis showed that the distance between ER and peroxisomal membranes increased in *pex11* cells, like in *pex32* cells (Fig. 6E). These data indicate that ER-localized Pex32 together with peroxisomal Pex11 contribute to the formation of peroxisome-ER contacts.

The absence of Pex32 does not affect PPV formation in *H. polymorpha pex3 atg1* cells

S. cerevisiae Pex30 and Pex31 are involved in the regulation of PPV formation. The absence of these proteins was reported to either stimulate (David et al., 2013; Mast et al., 2016) or delay (Joshi et al., 2016; Wang et al., 2018) PPV formation. Possibly, this relates to differences in assays that were used to monitor PPV formation. Using Pex14-GFP as a marker for PPVs, Joshi and colleagues showed that deletion of *PEX30* or *PEX31* resulted in a significant decrease in the number of Pex14-GFP spots in *S. cerevisiae pex3 atg1* cells (Joshi et al., 2016). A similar analysis in *H. polymorpha* revealed that deletion of *PEX32* in *pex3 atg1* cells did not alter the abundance of Pex14-GFP spots (Fig. 7A, B). CLEM analysis revealed that the Pex14-GFP spots in *pex3 atg1 pex32* cells represent clusters of small vesicles (Fig. 7C). As shown in Fig. 7D, *pex32 pex3 atg1* and *pex3 atg1* control cells contain morphologically very similar clusters of vesicles. These data indicate that *H. polymorpha* Pex32 does not play an important role in the regulation of PPV formation.

Discussion

Here, we show that all four members of the *H. polymorpha* Pex23 protein family (Pex23, Pex24, Pex29 and Pex32) localize to the ER. Of these, Pex32 and Pex24 predominantly accumulate at peroxisome-ER contacts and appeared to be very important for multiple peroxisome features. Pex23 is less important for peroxisomes, while we could not detect a peroxisomal phenotype in cells lacking Pex29. Possibly, Pex23 and Pex29 play redundant roles in peroxisome biology or are involved in other functions and hence do not represent true peroxins. Pex23 also accumulates at NVJs, suggesting that Pex23 family proteins may be intrinsic contact site proteins. Initial studies revealed that in *H. polymorpha pex23* and *pex29* cells, but not in *pex24* and *pex32* cells, mitochondrial morphology and lipid body abundance is altered, suggesting that these proteins may contribute to the formation of other organelles (Fei Wu, unpublished observations). Indeed, in *S. cerevisiae* ER domains enriched in Pex30 are the sites where most nascent lipid droplets form (Joshi et al., 2018).

Analysis of an evolutionary tree revealed that HpPex23 proteins can be partitioned in two major subgroups, one containing HpPex23 and HpPex32 and the other HpPex24 and HpPex29. There is no clear correlation between subgroup and molecular function, because the strongest peroxisomal phenotypes occurred in the absence of HpPex24 and HpPex32.

The absence of *H. polymorpha* Pex24 and Pex32 resulted in the loss of peroxisome ER contacts, accompanied by several peroxisome defects. These phenotypes could be suppressed by an artificial peroxisome ER tether protein, indicating that Pex24 and Pex32 function as contact site tethers. The peroxisomal membrane protein Pex11 also contributes to the formation of these contacts, however we do not know whether Pex11 contributes directly or indirectly to peroxisome-ER contact formation. Interestingly, *P pastoris* Pex11 pull down experiments resulted in the identification of Pex31, a member of the *P. pastoris* Pex23 protein family (Yan et al., 2008). Moreover, David and colleagues (David et al., 2013) identified ScPex11 as a specific binding partner in ScPex29 complexes, supporting the presence of Pex11 in protein complexes at peroxisome-ER contacts. *S. cerevisiae* Pex11 is also a component of a peroxisome-mitochondrion contact site, indicating that Pex11 contributes to the formation of different membrane contacts (Mattiazzi Ušaj et al., 2015).

Our data suggest that Pex24 and Pex32 are components of tether complexes that bridge peroxisomes to the ER. However, they do not meet all three criteria suggested for bona fide tethers by Eisenberg-Bord and colleagues (Eisenberg-Bord et al., 2016). These authors proposed that tethers (1) localize/accumulate in the contact site, (2) have the structural capacity to mediate binding to two opposing membranes and (3) exert a tethering force, which may among others be established by rescue by artificial tethers. Here we show that *H. polymorpha* Pex24 and Pex32 accumulate at peroxisome-ER contact sites (criterion 1) and that an artificial tether can rescue phenotypes caused by the absence of these proteins (criterion 3). Further studies are required to determine whether Pex24 and Pex32 also meet criterion 2.

The loss of peroxisome-ER contacts causes multiple phenotypes. It is not unprecedented that a contact site resident protein is involved in various processes. For instance the vacuolar membrane protein Vac8 functions in NVJs, vacuole fusion and inheritance in *S. cerevisiae* (Pan and Goldfarb, 1998). Also, the mitochondrial outer membrane protein Mdm10 is a component of ERMES and required for membrane protein insertion (Kornmann et al., 2009; Meisinger et al., 2004; Wiedemann and Pfanner, 2017).

A possible function of the Pex24-, Pex32- and Pex11-dependent peroxisome-ER contacts includes transfer of lipids from the ER to peroxisomes. Indeed, we observed reduced peroxisomal membrane surfaces in cells lacking Pex24 or Pex32. Yeast peroxisomes lack lipid biosynthetic enzymes hence expansion of the peroxisomal membrane relies on the supply of lipids from other sources. In *S. cerevisiae* peroxisomal membrane lipids may originate from multiple sources, including the mitochondrion, the Golgi apparatus, the vacuole and the ER (Flis et al., 2015; Rosenberger et al., 2009). Indeed, evidence for non-vesicular lipid transport between the ER and peroxisomes in yeast has been reported before (Raychaudhuri and Prinz, 2008).

In glucose-grown *H. polymorpha* cells the single peroxisome invariably associates with the edge of cortical ER sheets, where the ER is highly curved (Wu et al., 2019). Using CLEM we showed that Pex32 specifically localizes to these regions. This is consistent with studies in *S. cerevisiae*, which revealed that members of the Pex23 family occur in complexes with the ER-shaping reticulons, Rtn1/Rtn2, and Yop1(David et al., 2013; Joshi et al., 2016; Mast et al., 2016). ER-shaping proteins have been implicated in lipid exchange between the ER and mitochondria in *S. cerevisiae* (Voss et al., 2012). Therefore, it is tempting to speculate that highly curved ER regions where *H. polymorpha* Pex24 and Pex32 localize function in lipid transport. Also, like *S. cerevisiae* Pex30 and Pex31, HpPex23 family proteins have a reticulon-like domain and thus may have membrane shaping properties (Joshi et al., 2016). Peroxisome-ER contact sites that contribute to phospholipid transport recently have been identified in mammals as well. At these sites, the ER proteins VAPA/B interact with the peroxisome membrane proteins ACBD4/5 (Costello et al., 2017a,b; Hua et al., 2017).

Another role of peroxisome-ER contacts may be in peroxisome fission. Mitochondrion-ER contacts are important in the selection of fission sites (Friedman et al., 2011). A comparable mechanism may occur for peroxisomes. This is suggested by the presence of enlarged peroxisomes in *pex24* and *pex32* cells, similar as in *pex11* cells, which are known to be defective in peroxisome fission (Williams et al., 2015). A possible alternative explanation for the enlarged peroxisomes in *H. polymorpha pex23*, *pex24* and *pex32* cells is a change in membrane lipid composition, which may interfere with peroxisome fission. Although the absence of *S. cerevisiae* Pex30 changed the ER phospholipid composition (Wang et al., 2018), it is yet unknown whether this peroxin influences the phospholipid content of the peroxisomal membrane.

The peroxisome-ER contacts described in this study also contribute to peroxisome positioning at the cell cortex and proper segregation of the organelles over mother cells and buds. So far, only yeast Inp1 was implicated in peroxisome retention (Fagarasanu et al., 2005; Krikken et al., 2009). We here show that HpPex24 contributes to peroxisome retention in mother cells as well. We previously reported that *H. polymorpha pex11* cells show a peroxisome retention defect, underscoring a role of Pex11 in the formation of peroxisome-ER contacts (Krikken et al., 2009).

Proteins of the Pex23 family are implicated in the regulation of PPV formation, but are not required for their formation. Using different experimental approaches, the absence of *S. cerevisiae* Pex30 or Pex31 was shown to stimulate (David et al., 2013; Mast et al., 2016) or delay (Joshi et al., 2016; Wang et al., 2018) PPV formation. We here show that in *H. polymorpha* deletion of *PEX32* in *pex3 atg1* cells has no major effect on the abundance or morphology of PPVs, suggesting that *H. polymorpha* Pex32 does not play an important role in the regulation of PPV formation.

In conclusion, our data indicate that Pex24 and Pex32 contribute to tethering peroxisomes to the ER at membrane contact sites. These contacts play multiple functions, including in peroxisome biogenesis, membrane growth, organelle proliferation and segregation.

Materials and methods

Strains and growth conditions

The *H. polymorpha* strains used in this study are listed in Table S2. Yeast cells were grown in batch cultures at 37°C on mineral media (MM) (Van Dijken et al., 1976) supplemented with 0.5% glucose, 0.5% methanol or a mixture of 0.5% methanol and 0.05%

glycerol as carbon sources and 0.25% ammonium sulfate or 0.25% methylamine as nitrogen sources. When required, amino acids were added to the media to a final concentration of 30 µg/mL. Transformants were selected on YND plates (0.67% yeast nitrogen base without amino acids (YNB; Difco; BD) and 0.5% glucose) or on YPD plates (1% yeast extract, 1% peptone and 1% glucose) containing 2% agar supplemented with 100 µg/mL zeocin (Invitrogen), 300 µg/mL hygromycin B (Invitrogen) or 100 µg/ml nourseothricin (WERNER BioAgents).

Construction of *H. polymorpha* strains

The plasmids and primers used in this study are listed in Tables S3 and S4. All plasmid integrations were performed as described previously (Faber et al., 1994). All integrations were confirmed by PCR and all deletions were confirmed by PCR and southern blotting.

Construction of strains expressing Pex23-mGFP, Pex24-mGFP, Pex29-mGFP and Pex32-mGFP under control of the endogenous promoter

A plasmid encoding Pex23-mGFP was constructed as follows: a PCR fragment encoding the C-terminus of *PEX23* was obtained using primers Pex23 GFP-fw and Pex23 GFP-rev with *H. polymorpha* NCYC495 genomic DNA as a template. The obtained PCR fragment was digested with *Bgl*II and *Hin*dIII, and inserted between the *Bgl*II and *Hin*dIII sites of plasmid pHIPZ-mGFP fusinator. *Bsm*BI-linearized pHIPZ *PEX23*-mGFP was transformed into *yku80* cells, producing strain Pex23-mGFP.

The same methods were used to construct Pex24-mGFP, Pex29-mGFP and Pex32-mGFP strains. PCR was performed on WT genomic DNA with primers Pex24 fw and Pex24 rev to get C-terminus of *PEX24*, primers Pex29 fw and Pex29 rev were used for PCR to get C-terminus of *PEX29*, primers Pex32 fw and Pex32 rev were used for PCR to get C-terminus of *PEX32*. The obtained PCR fragment of *PEX24* was digested with *Bgl*II and *Hin*dIII, the PCR fragment of *PEX29* and the PCR fragment of *PEX32* were restricted by *Bam*HI and *Hin*dIII, these three digested fragments were inserted between the *Bgl*II and *Hin*dIII sites of pHIPZ-mGFP fusinator plasmid, respectively. *Bcl*I-linearized pHIPZ *PEX24*-mGFP, *Nru*I-linearized pHIPZ *PEX29*-mGFP and *Mfe*I-linearized pHIPZ *PEX32*-mGFP were transformed into *yku80* cells separately, producing strains Pex24-mGFP, Pex29-mGFP and Pex32-mGFP. *Mun*I-linearized pHIPH *PEX14*-mKate2 was transformed into Pex23-mGFP, Pex24-mGFP, Pex29-mGFP and Pex32-mGFP cells for colocalization study.

For the co-localization of Pex23 family proteins with the ER: *Dra*I-linearized pHIPX7 BiP$_{N30}$-mCherry-HDEL was integrated into Pex24-mGFP and Pex29-mGFP cells, respectively. *Stu*I-linearized pHIPX7 BiP$_{N30}$-mCherry-HDEL was transformed into Pex23-mGFP cells and Pex32-mGFP cells, respectively. Plasmid pHIPX7 BiP$_{N30}$-mCherry-HDEL was constructed as follows: first, a PCR fragment containing *BiP* was obtained with primers KN18 and KN19 using WT genomic DNA as templates. The obtained fragment was digested with *Bam*HI and *Hin*dIII, inserted between the *Bam*HI and *Hin*dIII sites of pBlueScript II, resulting in plasmid pBS-BiP. Then a PCR fragment containing GFP-HDEL was obtained with primers KN14 and KN17 using pANL29 as templates, the resulting fragment was digested with *Sal*I and *Bgl*II, and then inserted between the *Sal*I and *Bgl*II sites of pBS-BiP, resulting in pBS-BiP$_{N30}$-GFP-HDEL. Subsequently, pBS-BiP$_{N30}$-GFP-HDEL was digested with *Bam*HI/*Sal*I and inserted between the *Bam*HI/*Sal*I sites of pHIPX7 to obtain pHIPX7 BiP$_{N30}$-GFP-HDEL. Plasmid pHIPX7 BiP$_{N30}$-GFP-HDEL was digested with *Bam*HI/*Eco*RI and inserted between the *Bam*HI/*Eco*RI sites of pHIPX4, resulting in pHIPX4 BiP$_{N30}$-GFP-HDEL. *Not*I and *Sal*I were used to digest pHIPX4 BiP$_{N30}$-GFP-HDEL and inserted between the *Not*I and *Sal*I sites of pHIPZ4 DsRed-SKL to obtain plasmid pRSA017. Later, a PCR fragment was obtained by primers BIPmCh1_fw and BIPmCh1_rev on plasmid pMCE02, the resulting fragment was inserted between *Bgl*II and *Sal*I sites of pRSA017 to obtain pHIPZ4 BiP$_{N30}$-mCherry-HDEL. Finally, a PCR fragment was obtained by primers BIPmCh2_fw and BIPmCh1_rev using plasmid pHIPZ4 BiP$_{N30}$-mCherry-HDEL as a template, the resulting fragment was inserted between *Bgl*II and *Sal*I sites of pHIPX7 BiP$_{N30}$-GFP-HDEL, resulting in pHIPX7 BiP$_{N30}$-mCherry-HDEL.

Construction of strains producing Pex23-mGFP, Pex24-mGFP, Pex29-mGFP and Pex32-mGFP under control of the P_{AMO}

A plasmid encoding Pex24-mGFP behind the inducible promoter amine oxidase was constructed as follows: a PCR fragment containing *PEX24*-mGFP was obtained using primers

Pex24GFP fw and Pex24GFP rev with Pex24-mGFP genomic DNA as template. This PCR product and pHIPH5 were restricted by *Sbf*I and *Bam*HI and ligated which resulted in pHIPH5 *PEX24*-mGFP. *Pml*I-linearized pHIPH5 *PEX24*-mGFP was transformed into *yku80* or *pex32*::DsRed-SKL cells resulting in strain P_{AMO}Pex24-mGFP or strain *pex32*::DsRed-SKL::P_{AMO}Pex24-mGFP. Plasmid pHIPH5 was constructed by *Not*I and *Sph*I digested pHIPZ5, inserted into the *Not*I and *Sph*I sites of pHIPH4.

The plasmid pHIPH5 *PEX29*-mGFP and plasmid pHIPH5 *PEX32*-mGFP were constructed in the same way. Primers Pex29ov-fw and Pex29ov-rev were used to get a PCR fragment containing *PEX29*-mGFP with Pex29-mGFP genomic DNA as the template. Primers Pex32ov-fw and Pex32ov-rev were used to get a PCR fragment containing *PEX32*-mGFP with Pex32-mGFP genomic DNA as the template. PCR products of *PEX29*-mGFP and *PEX32*-mGFP were restricted by *Sbf*I and *Bcl*I, and insert between the *Sbf*I and *Bcl*I sites of pHIPH5 *PEX24*-mGFP, respectively, to get plasmid pHIPH5 *PEX29*-mGFP and pHIPH5 *PEX32*-mGFP. *Nar*I-linearized pHIPH5 *PEX29*-mGFP and pHIPH5 *PEX32*-mGFP were integrated into *yku80* or *pex32*::DsRed-SKL cells separately to overproduce Pex29-mGFP and Pex32-mGFP.

The plasmid of pHIPH5 *PEX23*-mGFP was constructed in two steps: first, a PCR fragment containing partial (no start codon) *PEX23*-mGFP was obtained using primers Pex23ov-fw and Pex23ov-rev with Pex23-mGFP genomic DNA as a template. PCR product and pHIPH5 *PEX24*-mGFP were restricted by *Sbf*I and *Bam*HI, ligated to produce pHIPH5 *PEX23p*-mGFP. Next, a PCR using primers Pex23ov2-fw and Pex23ov2-rev to obtain the left partial (with start codon) *PEX23*-mGFP fragment with plasmid pHIPH5 *PEX24*-mGFP as templates. PCR product and pHIPH5 *PEX23p*-mGFP were restricted by *Not*I and *Bam*HI, ligated to produce pHIPH5 *PEX23*-mGFP. *Nar*I-linearized pHIPH5 *PEX23*-mGFP was transformed into *yku80* or *pex32*::DsRed-SKL cells to overproduce Pex23-mGFP.

*Eco*RI-linearized pHIPN18 DsRed-SKL was integrated into *yku80*, P_{AMO}Pex23-mGFP, P_{AMO}Pex24-mGFP, P_{AMO}Pex29-mGFP, P_{AMO}Pex32-mGFP cells, respectively. A plasmid encoding pHIPN18 DsRed-SKL was constructed as follows: a vector fragment was obtained by *Hin*dIII and *Sal*I digestion of pHIPN18 GFP-SKL, whereas the DsRed-SKL insertion fragment was obtained by *Hin*dIII and *Sal*I digestion of pHIPZ4 DsRed-SKL, ligation resulted in the plasmid pHIPN18 DsRed-SKL. Plasmid pHIPN18 GFP-SKL was constructed as follow: *Not*I and *Xba*I digested pAMK94 inserted into the *Not*I and *Xba*I sites of pHIPN4 to get pHIPN18 GFP-SKL. Plasmid pAMK94 was constructed as follow: a PCR fragment containing *ADH1* was amplified with primers ADH1 fw and ADH1 rev with WT genomic DNA as template. *Not*I and *Hin*dIII digested PCR product was inserted into *Not*I and *Hin*dIII sites of pHIPZ4 eGFP-SKL.

*Mun*I-linearized pHIPN *VAC8*-mKate2 was integrated into Pex23-mGFP and P_{AMO}Pex24GFP cells to produce Vac8-mKate2. Plasmid pHIPN *VAC8*-mKate2 was constructed by fragment ligation from *Hin*dIII/*Sal*I digested plasmid pHIPZ *VAC8*-mKate2 and *Hin*dIII/*Sal*I digested plasmid pHIPN *PEX14*-mCherry. Plasmid pHIPZ *VAC8*-GFP and plasmid pHIPZ *PEX14*-mKate2 were digested with *Hin*dIII and *Bgl*II and ligated to obtain plasmid pHIPZ *VAC8*-mKate2. Plasmid pHIPZ *VAC8*-GFP was constructed by amplification of the *VAC8* gene, lacking the stop codon, using primers Vac8_BglII R and Vac8_F and genomic DNA as template. The resulting PCR product was digested with *Hin*dIII and *Bgl*II, and ligated between the *Hin*dIII and *Bgl*II sites of the pHIPZ-mGFP fusinator plasmid.

Construction of *pex23*, *pex24*, *pex29* and *pex32* deletion strains

The *pex23* deletion strain was constructed by replacing the *PEX23* region with the zeocin resistance gene as follows: first, a PCR fragment containing the zeocin resistance gene and 50 bp of the *PEX23* flanking regions were amplified with primers PEX23-Fw and PEX23-Rev using plasmid pENTR221-zeocin as template. The resulting *PEX23* deletion cassette was transformed into *yku80* cells to obtain strain *pex23*. *PEX24*, *PEX29* and *PEX32* were also replaced by the zeocin resistance gene in the same way. Primers for *PEX24* deletion cassette were PEX24-Fw and PEX24-Rev, primers for *PEX29* deletion cassette were dPEX29-F and dPEX29-R, and primers for *PEX32* deletion cassette were dPEX32-F and dPEX32-R. These three deletion cassettes were transformed into *yku80* cells, respectively, producing *pex24*, *pex29* and *pex32*.

The *Stu*I-linearized pHIPN7 GFP-SKL was transformed into *pex23* and *pex24* mutant cells separately to produce GFP-SKL. The *Ahd*I-linearized pFEM35 was transformed into *yku80*, *pex29* and *pex32* mutant cells, respectively, producing GFP-SKL.

The *Mun*I-linearized pHIPN *PMP47*-mGFP plasmid was transformed into *pex23*, *pex24*, *pex29* and *pex32* cells, respectively. Plasmid pHIPN *PMP47*-mGFP was constructed as follows: a PCR fragment encoding the nourseothricin resistance gene was obtained with primers Nat-fwd and Nat-rev using plasmid pHIPN4 as a template. The obtained PCR fragment was digested with *Not*I and *Xho*I and inserted between the *Not*I and *Xho*I sites of pMCE7, resulting in plasmid pHIPN *PMP47*-mGFP.

The *Dra*I-linearized pAMK15 was transformed into *pex32* cells to obtain a strain producing DsRed-SKL.

Construction of *pex23* family mutants with or without an artificial ERPER tether

To introduce an artificial peroxisome-ER tether, two plasmids pARM115 (pHIPH18 *PEX14*) and pARM118 (pHIPH18 *PEX14*-2HA-*UBC6*) were constructed as follows. A PCR fragment containing *PEX14* was amplified with primers Pex14-HindIII-fw and Pex14-PspXI-rev using the WT genomic DNA as a template. The PCR fragment was digested with *Hin*dIII and *Psp*XI, inserted between the *Hin*dIII and *Sal*I sites of pAMK94 to get plasmid pHIPZ18 *PEX14*. A *Not*I/*Bpi*I digested fragment from plasmid pHIPZ18 *PEX14* and a *Not*I/*Bpi*I digested fragment from plasmid pHIPH4 were ligated, resulting in plasmid pARM115. The *Age*I-linearized was transformed into *yku80*::GFP-SKL and *pex32*::GFP-SKL cells to produce P_{ADH1}Pex14 (Pex14++). A PCR fragment containing *PEX14*-2xHA was amplified by primers HindIII-Pex14 and Pex14-HA-HA. A fragment containing 2xHA-*UBC6* was amplified with primers HAHA-Ubc6 and Ubc6-PspXI and WT genomic DNA as template. The obtained PCR fragments were purified and used as templates together with primers HindIII-Pex14 and Ubc6-PspXI in a second PCR reaction. The obtained overlap PCR fragment was digested with *Hin*dIII and *Psp*XI, and inserted between the *Hin*dIII and *Sal*I sites of pAMK94, resulting in plasmid pARM053 (pHIPZ18 *PEX14*-2HA-*UBC6*). A *Not*I/*Bpi*I digested fragment from plasmid pAMK053 and a *Not*I/*Bpi*I digested fragment from plasmid pHIPH4 were ligated, resulting in plasmid pARM118. Then the *Age*I-linearized pARM118 was transformed into *yku80*::GFP-SKL, *yku80*::Pmp47-GFP, *pex23*::GFP-SKL, *pex24*::GFP-SKL, *pex24*::Pmp47-GFP, *pex29*::GFP-SKL, *pex32*::GFP-SKL and *pex32*::Pmp47-GFP cells, respectively, to produce P_{ADH1}Pex14-2HA-Ubc6 (ERPER).

Expression of Pex32-mGFP in different *pex* mutant cells

The *Bgl*II-linearized pHIPZ *PEX32*-mGFP were transformed into *pex3 atg1*::Pex14-mCherry, *pex5 atg1*::Pex14-mCherry, *pex11* and *pex25* cells, respectively, to produce Pex32-mGFP. *Blp*I-linearized pARM014 (pHIPX7 *PEX14*-mCherry) was transformed into *pex5 atg1* cells, which resulted in *pex5 atg1*::Pex14-mCherry. Plasmid pARM014 was constructed with following steps: first, a PCR fragment containing Pex14-mCherry was amplified with primers PRARM001 and PRARM002 using pSEM01 as a template. The obtained PCR fragment was digested with *Not*I and *Hin*dIII, and inserted between the *Not*I and *Hin*dIII sites of plasmid pHIPX7, resulting in plasmid pARM014. *ATG1* deletion cassette was amplified by PCR with primers pDEL-ATG1-fwd + pDEL-ATG1-rev and plasmid pARM011 as template. Then the PCR product integrated into *pex5* to get *pex5 atg1* mutant.

Two plasmids allowing disruption of *H. polymorpha PEX25* were constructed using Multisite Gateway technology as follows: First, the 5' and 3' flanking regions of the *PEX25* gene were amplified by PCR with primers RSAPex25-1+RSAPex25-2 and RSAPex25-3+RSAPex25-4, respectively, using *H. polymorpha* NCYC495 genomic DNA as a template. The resulting fragments were then recombined in donor vectors pDONR P4-P1R and pDONR P2R-P3, resulting in plasmids pENTR-PEX25 5' and pENTR-PEX25 3', respectively. Then, PCR amplification was performed using primers attB1-Ptef1-forward and attB2-Ttef1-reverse using pHIPN4 as the template. The resulting PCR fragment was recombined into vector pDONR-221 yielding entry vector pENTR-221-NAT. Recombination of the entry vectors pENTR-PEX25 5', pENTR-221-NAT, and pENTR-PEX25 3', and the destination vector pDEST-R4-R3, resulted in pRSA018. Then *PEX25* disruption cassette containing neursothricin resistance gene was amplified with primers RSAPex25-5 and RSAPex25-6 using pRSA018 as a template. To create *pex25*, the *PEX25* disruption cassette was transformed into *yku80* cells. *Blp*I-linearized pHIPH *PEX14*-mCherry was integrated into *pex11*::Pex32-mGFP or *pex25*::Pex32-mGFP to produce Pex14-mCherry.

Construction of *pex32 inp1* double and *pex3 atg1 pex32* triple deletion strains

To construct *pex32 inp1* mutant, a PCR fragment containing *INP1* deletion cassette was amplified with primers dInp1FW-F and dInp1-REV using plasmid pHIPH5 as a template. The resulting *INP1* deletion cassette was transformed into *pex32* cells to get double deletion of *pex32 inp1*. The *Ahd*I-linearized pFEM35 was transformed into *pex32 inp1* to produce GFP-SKL.

To construct *pex3 atg1 pex32* strain, a PCR fragment containing *PEX32* deletion cassette was amplified with primers dPex32-F and dPex32-R using *pex32* genomic DNA as a template. The resulting *PEX32* deletion cassette was transformed into *pex3 atg1* cells to get triple mutant of *pex3 atg1 pex32*. *Xho*I-linearized pHIPN-*PEX14*-mGFP plasmid was integrated into *pex3 atg1 pex32* cells.

A plasmid encoding pHIPN *PEX14*-mGFP was constructed as follows: a PCR fragment containing the nourseothricin resistance gene was obtained using primers Nat fw and Nat rev with plasmid pHIPN4 as a template. The PCR product and pSNA12 were digested with *Nsi*I and *Not*I, then ligated to produce pHIPN *PEX14*-mGFP.

Molecular and biochemical techniques

DNA restriction enzymes were used as recommended by the suppliers (Thermo Fisher Scientific or New England Biolabs). Polymerase chain reactions (PCR) for cloning were carried out with Phusion High-Fidelity DNA Polymerase (Thermo Fisher Scientific). An initial selection of positive transformants by colony PCR was carried out using Phire polymerase (Thermo Fisher Scientific). For DNA and amino acid sequence analysis, the Clone Manager 5 program (Scientific and Educational Software, Durham, NC) was used.

For Western blot analysis, total cell extracts were prepared as described previously (Baerends et al., 2000). Samples in Fig. 2E were denatured in urea loading buffer. Blots were decorated using anti-GFP antibodies (sc-996, Santa Cruz Biotech; 1:2,000 dilution), anti-pyruvate carboxylase-1 (Pyc1) antibodies (Ozimek et al., 2007, 1:10,000 dilution), anti-Pex14 antibodies (Komori et al., 1997, 1:10,000 dilution). Secondary goat anti-rabbit (31460) or goat anti-mouse (31430) antibodies conjugated to horseradish peroxidase (HRP) (Thermo

Scientific, 1:5,000 dilution) were used for detection. Blots were scanned by using a densitometer (GS-710; Bio-Rad Laboratories).

Fluorescence microscopy

Wide-field FM images of living cells and on cryosections for CLEM were captured at room temperature using a 100×1.30 NA objective (Carl Zeiss, Oberkochen, Germany). Images were obtained from the cells in growth media using a fluorescence microscope (Axioscope A1; Carl Zeiss), Micro-Manager 1.4 software and a digital camera (Coolsnap HQ^2; Photometrics). The GFP fluorescence were visualized with a 470/40 nm band-pass excitation filter, a 495 nm dichromatic mirror, and a 525/50 nm band-pass emission filter. DsRed fluorescence were visualized with a 546/12 nm band-pass excitation filter, a 560 nm dichromatic mirror, and a 575-640 nm band-pass emission filter. mCherry and mKate2 fluorescence were visualized with a 587/25 nm band-pass excitation filter, a 605 nm dichromatic mirror, and a 670/70 nm band-pass emission filter.

Confocal images were captured with an LSM800 Airyscan confocal microscope (Carl Zeiss) using Zen 2.3 software (Carl Zeiss) and a 100x/1.40 plan apochromat objective and GaAsP detectors. For quantitative analysis of peroxisomes or Pex14-mGFP fluorescent spots, z-stacks were made of randomly chosen fields.

Image analysis was performed using ImageJ, all bright field images have been adjusted to only show cell outlines. Figures were prepared using Adobe Illustrator software.

Electron microscopy

For morphological analysis, cells were fixed in 1.5% potassium permanganate, post-stained with 0.5% uranyl acetate and embedded in Epon. Image analysis and distance measurements are performed using ImageJ. For the quantification of the ER, the total length of the plasma membrane and the peripheral ER was measured from cell sections and from this the percentage of the cortex covered by the ER was calculated. Correlative light and electron microscopy (CLEM) was performed using cryo-sections as described previously (Knoops et al., 2015). After fluorescence imaging, the grid was post-stained and embedded in a mixture of 0.5% uranyl acetate and 0.5% methylcellulose. Acquisition of the double-tilt tomography series was performed manually in a CM12 TEM running at 100 kV and included a tilt range of 40° to −40 with 2.5° increments. To construct the CLEM images, pictures taken with FM and EM were aligned using the eC-CLEM plugin in Icy (Paul-Gilloteaux et al., 2017) (http://icy.bioimageanalysis.org). Reconstruction of the tomograms was performed using the IMOD software package.

Immuno-EM was performed as described previously (Thomas et al., 2018). Labeling of HA was performed using monoclonal antibodies (Sigma-Aldrich H9658; 1:100 dilution) followed by goat-anti-mouse antibodies conjugated to 6 nm gold (Aurion, the Netherlands; 1:20 dilution).

In silico analyses

Homologous sequences were detected using BLASTP with an e-value of 1e-5 (Altschul et al., 1990). Linear and secondary structure predictions were realized using Foundation (Bordin et al., 2018).

Phylogenetic tree

The multiple sequence alignment used as input was created using ClustalOmega (Sievers et al., 2011) with default parameters and manually curated in Jalview (Waterhouse et al., 2009). The tree was generated using PhyML 3.1 (Guindon et al., 2010) using the LG matrix, 100 bootstraps, tree and leaves refinement, SPR moves, and amino acids substitution rates determined empirically.

Peroxisome membrane surface area calculation

For peroxisome membrane surface area calculation: average peroxisome volume (V) and average peroxisome number per cell (N) were determined using a plugin for ImageJ (Thomas et al., 2015) from two independent experiments (2x300 cells were counted). Formula $V = \frac{4}{3}\pi r^3$ was used to calculate peroxisome radius (r) and formula $S = 4\pi r^2$ was used to calculate the average peroxisome surface area. The average peroxisome number per cell *N* multiplied with *S* is the peroxisome membrane surface area per cell.

Quantification of the distance between GFP spots and cell cortex

For the calculation of the distance between the GFP-SKL spot and the cell cortex, cells containing GFP spots were selected and processed by ImageJ. Subsequently, the distance between the middle of the GFP spot and the cell outline was measured. For cells containing two or more GFP spots, only the spot that is closest to the cell outline was used.

Peroxisome inheritance quantification

Peroxisome inheritance quantification was performed using the same method as published previously (Krikken et al., 2009).

Author contributions

FW, AA, AMK, RdB and IvdK conceived the project; FW, AA, AMK, RdB, NB, DPD, IJvdK performed the experiments, analysed the data and prepared the figures; FW, IJvdK wrote the original draft. All contributed to reviewing and editing the manuscript.

Acknowledgements

We thank Benjan Karnebeek, Malgorzata Krygowska and Kim van Maldegem for assistance in strain construction and Tim Levine (University College London, UK) for advice in protein sequence analysis.

Funding sources and disclosure of conflicts of interest

This work was supported by a grant from the Marie Curie Initial Training Networks (ITN) program PerFuMe (Grant Agreement Number 316723) to NB, DPD and IvdK, the CHINA SCHOLARSHIP COUNCIL (CSC) to FW and the Netherlands Organisation for Scientific Research/Chemical Sciences (NWO/CW) to AA (711.012.002).

The authors declare no competing financial interests.

References

Altschul, S. F., Gish, W., Miller, W., Myers, E. W., and Lipman, D. J. (1990). Basic local alignment search tool. *J. Mol. Biol.* **215**, 403–410.

Baerends, R. J. S., Faber, K. N., Kram, A. M., Kiel, J. A. K. W., van der Klei, I. J., and Veenhuis, M. (2000). A stretch of positively charged amino acids at the N terminals of Hansenula polymorpha Pex3p is involved in incorporation of the protein into the peroxisomal membrane. *J. Biol. Chem.* **275**, 9986–9995.

Bansal, D., and Campbell, K. P. (2004). Dysferlin and the plasma membrane repair in muscular dystrophy. *Trends Cell Biol.* **14**, 206–213.

Bansal, D., Miyake, K., Vogel, S. S., Groh, S., Chen, C.-C., Williamson, R., McNeil, P. L., and Campbell, K. P. (2003). Defective membrane repair in dysferlin-deficient muscular dystrophy. *Nature* **423**, 168–172.

Bordin, N., González-Sánchez, J. C., and Devos, D. P. (2018). PVCbase: An integrated web resource for the PVC bacterial proteomes. *Database* **2018**, 1–10.

Brown, T. W., Titorenko, V. I., and Rachubinski, R. A. (2000). Mutants of the *Yarrowia lipolytica PEX23* Gene Encoding an Integral Peroxisomal Membrane Peroxin Mislocalize Matrix Proteins and Accumulate Vesicles Containing Peroxisomal Matrix and Membrane Proteins. *Mol. Biol. Cell* **11**, 141–152.

Costello, J. L., Castro, I. G., Hacker, C., Schrader, T. A., Metz, J., Zeuschner, D., Azadi, A. S., Godinho, L. F., Costina, V., Findeisen, P., et al., and Schrader, M. (2017). ACBD5 and VAPB mediate membrane associations between peroxisomes and the ER. *J. Cell Biol*. **216**, 331–342.

Costello, J. L., Castro, I. G., Schrader, T. A., Islinger, M., and Schrader, M. (2017). Peroxisomal ACBD4 interacts with VAPB and promotes ER-peroxisome associations. *Cell Cycle* **16**, 1039–1045.

David, C., Koch, J., Oeljeklaus, S., Laernsack, A., Melchior, S., Wiese, S., Schummer, A., Erdmann, R., Warscheid, B., and Brocard, C. (2013). A Combined Approach of Quantitative Interaction Proteomics and Live-cell Imaging Reveals a Regulatory Role for Endoplasmic Reticulum (ER) Reticulon Homology Proteins in Peroxisome Biogenesis. *Mol. Cell. Proteomics* **12**, 2408–2425.

Distel, B., Erdmann, R., Gould, S. J., Blobel, G., Crane, D. I., Cregg, J. M., Dodt, G., Fujiki, Y., Goodman, J. M., Just, W. W., et al., and Veenhuis, M. (1996). A unified nomenclature for peroxisome biogenesis factors. *J. Cell Biol.* **135**, 1–3.

Eisenberg-Bord, M., Shai, N., Schuldiner, M., and Bohnert, M. (2016). A Tether Is a Tether Is a Tether: Tethering at Membrane Contact Sites. *Dev. Cell* **39**, 395–409.

Faber, K. N., Haima, P., Harder, W., Veenhuis, M., and Ab, G. (1994). Highly-efficient electrotransformation of the yeast Hansenula polymorpha. *Curr. Genet.* **25**, 305–310.

Fagarasanu, M., Fagarasanu, A., Tam, Y. Y. C., Aitchison, J. D., and Rachubinski, R. A. (2005). Inp1p is a peroxisomal membrane protein required for peroxisome inheritance in Saccharomyces cerevisiae. *J. Cell Biol.* **169**, 765–775.

Flis, V. V., Fankl, A., Ramprecht, C., Zellnig, G., Leitner, E., Hermetter, A., and Daum, G. (2015). Phosphatidylcholine supply to peroxisomes of the yeast Saccharomyces cerevisiae. *PLoS One* **10**, 1–19.

Friedman, J. R., Lackner, L. L., West, M., DiBenedetto, J. R., Nunnari, J., and Voeltz, G. K. (2011). ER tubules mark sites of mitochondrial division. *Science* **334**, 358–362.

Guindon, S., Dufayard, J. F., Lefort, V., Anisimova, M., Hordijk, W., and Gascuel, O. (2010). New algorithms and methods to estimate maximum-likelihood phylogenies: Assessing the performance of PhyML 3.0. *Syst. Biol.* **59**, 307–321.

Hua, R., Cheng, D., Coyaud, É., Freeman, S., Pietro, E. Di, Wang, Y., Vissa, A., Yip, C. M., Fairn, G. D., Braverman, N., et al., and Kim, P. K. (2017). VAPs and ACBD5 tether peroxisomes to the ER for peroxisome maintenance and lipid homeostasis. *J. Cell Biol*. **216**, 367-377.

Joshi, A. S., Huang, X., Choudhary, V., Levine, T. P., Hu, J., and Prinz, W. A. (2016). A family of membrane-shaping proteins at ER subdomains regulates pre-peroxisomal vesicle biogenesis. *J. Cell Biol.* **215**, 515–529.

Joshi, A. S., Nebenfuehr, B., Choudhary, V., Satpute-Krishnan, P., Levine, T. P., Golden, A., and Prinz, W. A. (2018). Lipid droplet and peroxisome biogenesis occur at the same ER subdomains. *Nat. Commun*. **9**, 2940.

Kiel, J. A. K. W., Veenhuis, M., and van der Klei, I. J. (2006). PEX genes in fungal genomes: Common, rare or redundant. *Traffic* **7**, 1291–1303.

Knoblach, B., Sun, X., Coquelle, N., Fagarasanu, A., Poirier, R. L., and Rachubinski, R. A. (2013a). An ER-peroxisome tether exerts peroxisome population control in yeast. *EMBO J.* **32**, 2439–2453.

Knoops, K., de Boer, R., Kram, A., and Van Der Klei, I. J. (2015). Yeast pex1 cells contain peroxisomal ghosts that import matrix proteins upon reintroduction of Pex1. *J. Cell Biol.* **211**, 955–962.

Knoops, K., Manivannan, S., Cepińska, M. N., Krikken, A. M., Kram, A. M., Veenhuis, M., and van der Klei, I. J. (2014). Preperoxisomal vesicles can form in the absence of Pex3. *J. Cell Biol.* **204**, 659–668.

Komori, M., Rasmussen, S. W., Kiel, J. A. K. W., Baerends, R. J. S., Cregg, J. M., Van Der Klei, I. J., and Veenhuis, M. (1997). The Hansenula polymorpha PEX14 gene encodes a novel peroxisomal membrane protein essential for peroxisome biogenesis. *EMBO J.* **16**, 44–53.

Kornmann, B., Currie, E., Collins, S. R., Schuldiner, M., Nunnari, J., Weissman, J. S., and Walter, P. (2009). An ER-Mitochondria Tethering Complex Revealed by a Synthetic Biology Screen. *Science* **325**, 477–481.

Krikken, A. M., Veenhuis, M., and van der Klei, I. J. (2009). Hansenula polymorpha pex11 cells are affected in peroxisome retention. *FEBS J.* **276**, 1429–1439.

Lv, X., Liu, J., Qin, Y., Liu, Y., Jin, M., Dai, J., Chua, B. T., Yang, H., and Li, P. (2019). Identification of gene products that control lipid droplet size in yeast using a high-throughput quantitative image analysis. *Biochim. Biophys. Acta - Mol. Cell Biol. Lipids* **1864**, 113-127.

Ma, W., and Goldberg, J. (2013). Rules for the recognition of dilysine retrieval motifs by coatomer. *EMBO J.* **32**, 926–937.

Mast, F. D., Jamakhandi, A., Saleem, R. A., Dilworth, D. J., Rogers, R. S., Rachubinski, R. A., and Aitchison, J. D. (2016). Peroxins Pex30 and Pex29 dynamically associate with reticulons to regulate peroxisome biogenesis from the endoplasmic reticulum. *J. Biol. Chem.* **291**, 15408–15427.

Mattiazzi Ušaj, M., Brložnik, M., Kaferle, P., Žitnik, M., Wolinski, H., Leitner, F., Kohlwein, S. D., Zupan, B., and Petrovič, U. (2015). Genome-wide localization study of yeast pex11 identifies peroxisome-mitochondria interactions through the ERMES complex. *J. Mol. Biol*. **427**, 2072-2087.

Meisinger, C., Rissler, M., Chacinska, A., Szklarz, L. K. S., Milenkovic, D., Kozjak, V., Schönfisch, B., Lohaus C., Meyer H, E., Yaffe, M. P., and Pfanner, N. (2004). The Mitochondrial Morphology Protein Mdm10 Functions in Assembly of the Preprotein Translocase of the Outer Membrane. *Dev. Cell* **7**, 61–71.

North, K. N., Lek, A., Evesson, F. J., Sutton, R. B., and Cooper, S. T. (2011). Ferlins: Regulators of Vesicle Fusion for Auditory Neurotransmission, Receptor Trafficking and Membrane Repair. *Traffic* **13**, 185–194.

Ozimek, P. Z., Klompmaker, S. H., Visser, N., Veenhuis, M., and van der Klei, I. J. (2007). The transcarboxylase domain of pyruvate carboxylase is essential for assembly of the peroxisomal flavoenzyme alcohol oxidase. *FEMS Yeast Res.* **7**, 1082–1092.

Pan, X., and Goldfarb, D. S. (1998). YEB3/VAC8 encodes a myristylated armadillo protein of the Saccharomyces cerevisiae vacuolar membrane that functions in vacuole fusion and inheritance. *J. Cell Sci.* **111**, 2137–2147.

Paul-Gilloteaux, P., Heiligenstein, X., Belle, M., Domart, M.-C., Larijani, B., Collinson, L., Raposo, G., and Salamero, J. (2017). Erratum: Corrigendum: eC-CLEM: flexible multidimensional registration software for correlative microscopies. *Nat. Methods* **14**, 323–323.

Raychaudhuri, S., and Prinz, W. A. (2008). Nonvesicular phospholipid transfer between peroxisomes and the endoplasmic reticulum. *Proc. Natl. Acad. Sci.* **105**, 15785–15790.

Rosenberger, S., Connerth, M., Zellnig, G., and Daum, G. (2009). Phosphatidylethanolamine synthesized by three different pathways is supplied to peroxisomes of the yeast Saccharomyces cerevisiae. *Biochim. Biophys. Acta.* **1791**, 379–387.

Sievers, F., Wilm, A., Dineen, D., Gibson, T. J., Karplus, K., Li, W., Lopez, R., McWilliam, H., Remmert, M., Söding, J., et al., and Higgins, D. G. (2011). Fast, scalable generation of high-quality protein multiple sequence alignments using Clustal Omega. *Mol. Syst. Biol.* **7**, 539.

Tam, Y. Y. C., and Rachubinski, R. A. (2002). Yarrowia lipolytica Cells Mutant for the PEX24 Gene Encoding a Peroxisomal Membrane Peroxin Mislocalize Peroxisomal Proteins and Accumulate Membrane Structures Containing Both Peroxisomal Matrix and Membrane Proteins. *Mol. Biol. Cell* **13**, 2681–2691.

Thomas, A. S., Krikken, A. M., de Boer, R., and Williams, C. (2018). Hansenula polymorpha Aat2p is targeted to peroxisomes via a novel Pex20p-dependent pathway. *FEBS Lett*. **592**, 2466–2475.

Thomas, A. S., Krikken, A. M., van der Klei, I. J., and Williams, C. P. (2015). Phosphorylation of Pex11p does not regulate peroxisomal fission in the yeast Hansenula polymorpha. *Sci. Rep*. **5**, 1–11.

van der Klei, I. J., Yurimoto, H., Sakai, Y., and Veenhuis, M. (2006). The significance of peroxisomes in methanol metabolism in methylotrophic yeast. *Biochim. Biophys. Acta*. **1763**, 1453–1462.

Van Dijken, L. P., Otto, R., and Harder, W. (1976). Growth of Hansenula polymorpha in a methanol-limited chemostat. *Arch. Microbiol.* **111**, 137–144.

Vizeacoumar, F. J., Torres-Guzman, J. C., Bouard, D., Aitchison, J. D., and Rachubinski, R. A. (2004). Pex30p, Pex31p, and Pex32p Form a Family of Peroxisomal Integral Membrane Proteins Regulating Peroxisome Size and Number in Saccharomyces cerevisiae. *Mol. Biol. Cell* **15**, 665–677.

Vizeacoumar, F. J., Torres-Guzman, J. C., Tam, Y. Y. C., Aitchison, J. D., and Rachubinski, R. A. (2003). YHR150w and YDR479c encode peroxisomal integral membrane proteins involved in the regulation of peroxisome number, size, and distribution in Saccharomyces cerevisiae. *J. Cell Biol.* **161**, 321–332.

Voss, C., Lahiri, S., Young, B. P., Loewen, C. J., and Prinz, W. A. (2012). ER-shaping proteins facilitate lipid exchange between the ER and mitochondria in S. cerevisiae. *J. Cell Sci*. **125**, 4791–4799.

Wang, S., Idrissi, F. Z., Hermansson, M., Grippa, A., Ejsing, C. S., and Carvalho, P. (2018). Seipin and the membrane-shaping protein Pex30 cooperate in organelle budding from the endoplasmic reticulum. *Nat. Commun* **9**, 1–12.

Waterhouse, A. M., Procter, J. B., Martin, D. M. A., Clamp, M., and Barton, G. J. (2009). Jalview Version 2-A multiple sequence alignment editor and analysis workbench. *Bioinformatics* **25**, 1189–1191.

Wiedemann, N., and Pfanner, N. (2017). Mitochondrial Machineries for Protein Import and Assembly. *Annu. Rev. Biochem.* **86**, 685–714.

Williams, C., Opalinski, L., Landgraf, C., Costello, J., Schrader, M., Krikken, A. M., Knoops, K., Kram, A. M., Volkmer, R., and van der Klei, I. J. (2015). The membrane remodeling protein Pex11p activates the GTPase Dnm1p during peroxisomal fission. *Proc. Natl. Acad. Sci. U. S. A.* **112**, 6377–6382.

Wróblewska, J. P., Cruz-Zaragoza, L. D., Yuan, W., Schummer, A., Chuartzman, S. G., de Boer, R., Oeljeklaus, S., Schuldiner, M., Zalckvar, E., Warscheid, B., et al., and van der Klei, I. J. (2017). Saccharomyces cerevisiae cells lacking Pex3 contain membrane vesicles that harbor a subset of peroxisomal membrane proteins. *Biochim. Biophys. Acta Mol. Cell Res.* **1864**, 1656–1667.

Wu, H., de Boer, R., Krikken, A. M., Akşit, A., Yuan, W., and van der Klei, I. J. (2018). Peroxisome development in yeast is associated with the formation of Pex3-dependent peroxisome-vacuole contact sites. *Biochim. Biophys. Acta Mol. Cell Res.* **1866**, 349–359.

Wu, H. (2020). Pex3-mediated peroxisomal membrane contact sites in yeast. *PhD thesis*, University of Groningen, Groningen, the Netherlands.

Yan, M., Rachubinski, D. A., Joshi, S., Rachubinski, R. A., and Subramani, S. (2008). Dysferlin Domain-containing Proteins, Pex30p and Pex31p, Localized to Two Compartments, Control the Number and Size of Oleate-induced Peroxisomes in Pichia pastoris. *Mol. Biol. Cell* **19**, 885–898.

Legends to Figures

Figure 1. Yeast Pex23 family proteins. (A) Protein phylogeny. Protein sequences from *S. cerevisiae*, *H. polymorpha*, *P. pastoris* and *Y. lipolytica* were retrieved from NCBI-protein. Phylogenetic tree: numbers represent the bootstraps values, while branch length represents the amino acidic substitution rates. (B) Secondary structure features of *H. polymorpha* Pex23 proteins obtained with Foundation (Bordin et al., 2018). The black horizontal lines represent the protein sequence. The predicted β-strands and α-helices are depicted by bars above each line in cyan and magenta, with the height of the bars representing the confidence of the prediction. Transmembrane helices (TMH) predictions are depicted as green boxes underneath the secondary structure prediction. The Protein Data Bank (PDB) domain represents the DysF domain.

Figure 2. *H. polymorpha* Pex23 family proteins localize to the ER. FM images of glucose-grown *H. polymorpha* cells producing the indicated GFP fusion proteins under control of their endogenous promoters together with the peroxisomal marker Pex14-mKate2 (A) or the ER marker BiP-mCherry-HDEL (B). (A, B) The merged images show the cell contours in white. Graphs show relative fluorescence intensity along the dotted lines. Scale bar: 1 μm. Representative images of two experiments are shown. (C) FM images of glucose/methylamine-grown *H. polymorpha* WT cells producing the peroxisomal marker DsRed-SKL and the indicated GFP fusion proteins under control of the amine oxidase promoter (P_{AMO}). Scale bar: 1 μm. Representative images of two experiments are shown. (D) Co-localization of Vac8-mKate2 with Pex23-GFP produced under control of the endogenous promoter or Pex24-GFP expressed under control of the P_{AMO}. Scale bar: 1 μm. Representative images of two experiments are shown. (E) Western Blot analysis of the indicated strains. Cells were grown for 4 hours on glucose. Strains producing the GFP fusion proteins under control of the P_{AMO} were grown in media containing methylamine as nitrogen source. Equal amounts of cellular lysates were loaded per lane. Blots were decorated with □-GFP or α-Pyruvate carboxylase 1 (Pyc1) antibodies. Pyc1 was used as a loading control. A representative blot of three experiments is shown.

Figure 3. Deletion of *PEX23, PEX24* or *PEX32* results in aberrant peroxisome formation. FM (A) and CLSM (B) images in conjunction with peroxisome quantification of the indicated deletion strains producing the peroxisome matrix protein GFP-SKL and grown on glucose. Scale bar: 2 μm. The error bars represent s.d. from two independent experiments (*n*=2 using 500 cells from each experiment). (C) CLSM images of Pmp47-GFP producing cells grown on a mixture of glycerol and methanol. Scale bar: 2 μm. In the upper right corners of the graphs, the average number of peroxisomes per cell is indicated. The error bars represent s.d. from two independent experiments (*n*=2 using 300 cells from each experiment). (D) Growth curves of the indicated strains in media containing a mixture of glycerol and methanol. The optical density (Y-axis) is expressed as absorbance at 660 nm (OD_{660}). The error bars represent the s.d. (*n*=2) from two independent cultures.

Figure 4. Deletion of *PEX23, PEX24* or *PEX32* results in an increase in distance between peroxisomal and ER membranes. (A, B, C) EM images of thin sections of $KMnO_4$-fixed glucose-grown cells of the indicated strains and quantification of the distance between the ER and peroxisomal membranes. The error bar represents the s.d. from two independent experiments (*n*=2 based on 21 peroxisomes in random sections from each experiment). CW - cell wall; ER - endoplasmic reticulum; P - peroxisome; M - mitochondrion; N - nucleus. Scale bar: 200 nm. (D) Quantification of ER abundance at the cell cortex. The percentage of the cell cortex covered by the ER was measured in 20 random cell sections using EM. (E) FM images and a SuperPlot showing the distance between the GFP spot and the cell cortex in the indicated strains producing GFP-SKL. *n*=2 using 24 cells from each biological replicate. The duplicate experiments are color coded. The circles represent the single data points. The squares are the average from each experiment and the error bars indicate the s.d.. (F) Quantification of the presence of peroxisomes in both the mother cell and bud in the indicated mutants. The error bar represents the s.d. from two independent experiments (*n*=2 using 20 peroxisome containing budding yeast cells from each experiment).

Figure 5. Suppression of peroxisome defects by an artificial peroxisome-ER tether. (A) Schematic representation of the ERPER tethering. (B) Immunolabelling using HA antibodies

of a WT P_{ADH1}*PEX14-HAHA-UBC6* cell. M - mitochondrion; P - peroxisome; ER-endoplasmic reticulum. Cells were embedded for EM once and the labelling was performed twice. Scale bar: 200 nm. (C) EM images of $KMnO_4$-fixed cells of the indicated mutants strains producing ERPER. Scale bar in upper images is 500 nm and in bottom images is 200 nm. Cells were embedded for EM once. (D) Fluorescence microscopy analysis of the indicated strains grown on glycerol/methanol and producing GFP-SKL. Because peroxisomes harbor an alcohol oxidase crystalloid, GFP is not evenly distributed over the peroxisomal matrix. Scale bar: 2 μm. Representative images of two experiments are shown. (E) Quantification of peroxisome numbers based on CLSM analysis of methanol/glycerol grown PMP47-GFP producing cells of the indicated mutant strains containing ERPER. n=2 using 300 cells from two independent cultures were quantified. (F) Growth curves of the indicated strains on glycerol/methanol. Error bars indicate s.d. from two independent cultures. (G) Average cellular peroxisome surface area calculation based on CLSM images of methanol/glycerol-grown cells of the indicated strains. Error bars indicate s.d. from two independent experiments (n=2 using 300 cells from each experiment). (H) Quantification of the average abundance of peroxisomal membranes in 50 cell sections of the indicated strains from single experiment.

Figure 6. The specific Pex32 localization depends on Pex3 and Pex11. (A) FM images and peroxisome quantification of glucose-grown WT and *pex32* cells with or without overproduction of the indicated proteins. Peroxisomes are marked with DsRed-SKL. The error bars represent s.d. from two independent experiments (n=2 using 200 cells from each experiment). Scale bar: 2 μm. (B) Growth curves of the indicated strains in media containing a mixture of glycerol and methanol. The optical density (Y-axis) is expressed as absorbance at 660 nm (OD_{660}). The error bars represent s.d. (n=2) from two independent cultures. (C) CLEM of glucose/methylamine-grown cells producing DsRed-SKL and Pex32-GFP under control of the P_{AMO}. The upper row shows FM images of 150 nm thick cryo-sections. The lower row shows an overlay of FM and electron microscopy (EM) images of the same cell section. The region of interest is indicated (dashed box). A tomogram was reconstructed and 3D rendered. P - peroxisome: blue; ER: orange; plasma membrane: cyan. Scale bars: (FM

image) 2 μm, (EM images) 500 nm, or (3D) 200 nm. A representative of four tomograms is shown. (D) FM images of glucose-grown indicated *pex* mutant cells producing Pex32-GFP under control of their endogenous promoters together with the peroxisomal marker Pex14-mKate2. Scale bar: 2 μm. Representative images of three experiments are shown. (E) EM image of KMnO4-fixed glucose-grown *pex11* mutant cell (left) and the peroxisome-ER distance quantification in *PEX11* deletion strain (right). CW - cell wall; ER - endoplasmic reticulum; P - peroxisome; M - mitochondrion. The error bar represents s.d. from two independent experiments (*n*=2 using 20 cell sections from each experiment). Scale bar: 200 nm.

Figure 7. Deletion of *pex32* in *pex3 atg1* cells does not result in major alterations in PPV abundance or morphology. (A) CLSM images of glycerol/methanol grown cells producing Pex14-GFP as a PPV marker. Scale bar: 2 μm. Representative images of two experiments are shown. (B) Distribution of the number of Pex14-GFP spots per cell and the average number of spots per cell. (*n*=2 using 280 cells from two independent experiments) (C-I) Wide-field FM image of a thick cryo-section (250 nm) of *atg1 pex3 pex32* cells producing Pex14-GFP. (C-II) CLEM showing an overlay image of Pex14-GFP (FM) and the TEM micrograph of the same region indicated with the white dashed box in C-I. (C-III) Electron tomographic slice from a tomogram recorded at the region indicated in C-II. White arrows indicate the position of the PPVs. (C-IV) 3D rendered volume of the reconstructed tomogram. *Blue*- PPVs, *yellow*-vacuole, *magenta* - plasma membrane. Scale bars: (C-I) 2 μm, (C-II) 500 nm, or (C-III) 200 nm. (D) EM analysis of $KMnO_4$-fixed *atg1 pex3* (upper row) and *atg1 pex3 pex32* (bottom row) cells. II shows a higher magnification of the region indicated in I. Scale bars: (D-I) 500 nm, or (D-II) 200 nm.

A

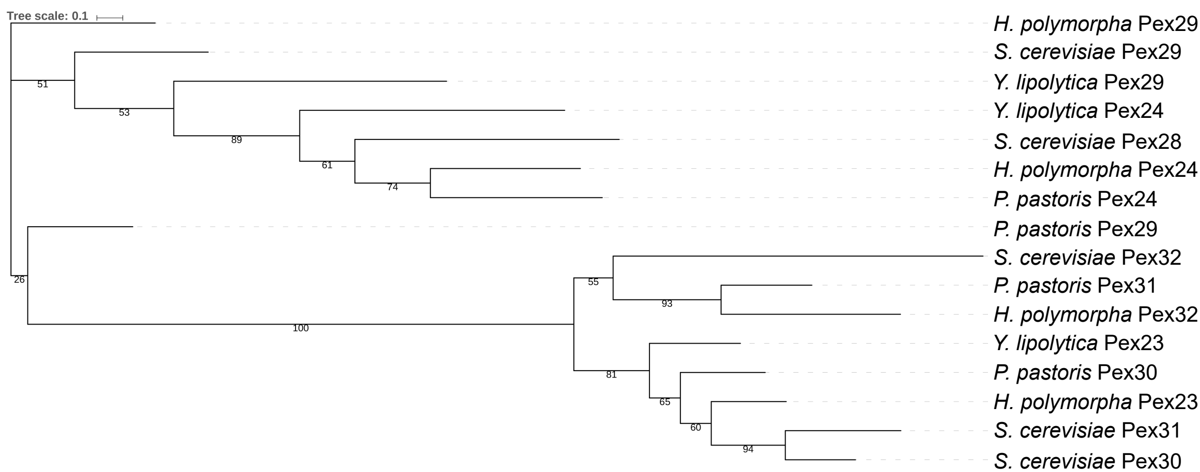
Tree scale: 0.1
H. polymorpha Pex29
S. cerevisiae Pex29
Y. lipolytica Pex29
Y. lipolytica Pex24
S. cerevisiae Pex28
H. polymorpha Pex24
P. pastoris Pex24
P. pastoris Pex29
S. cerevisiae Pex32
P. pastoris Pex31
H. polymorpha Pex32
Y. lipolytica Pex23
P. pastoris Pex30
H. polymorpha Pex23
S. cerevisiae Pex31
S. cerevisiae Pex30
51
53
89
61
74
26
100
55
93
81
65
60
94

B

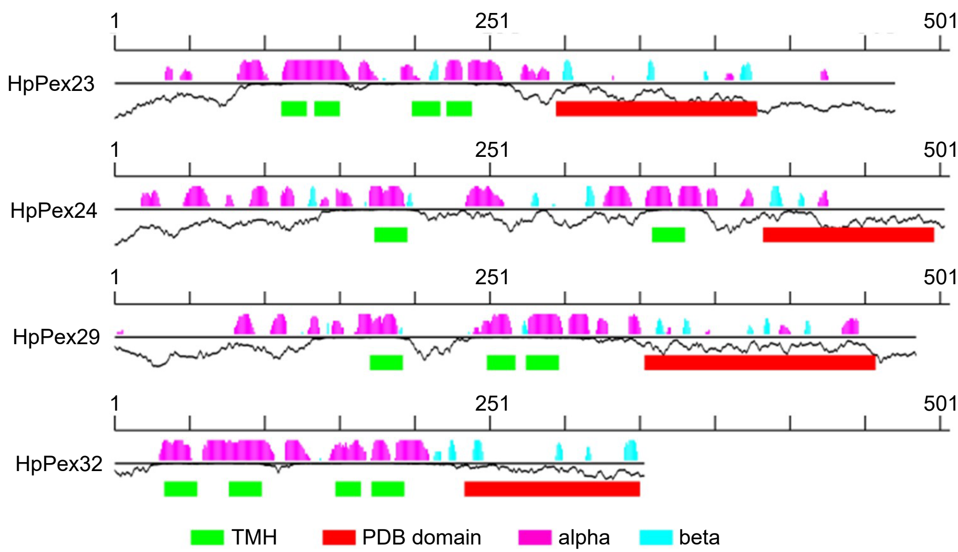
1
251
501
HpPex23
HpPex24
HpPex29
HpPex32
TMH
PDB domain
alpha
beta

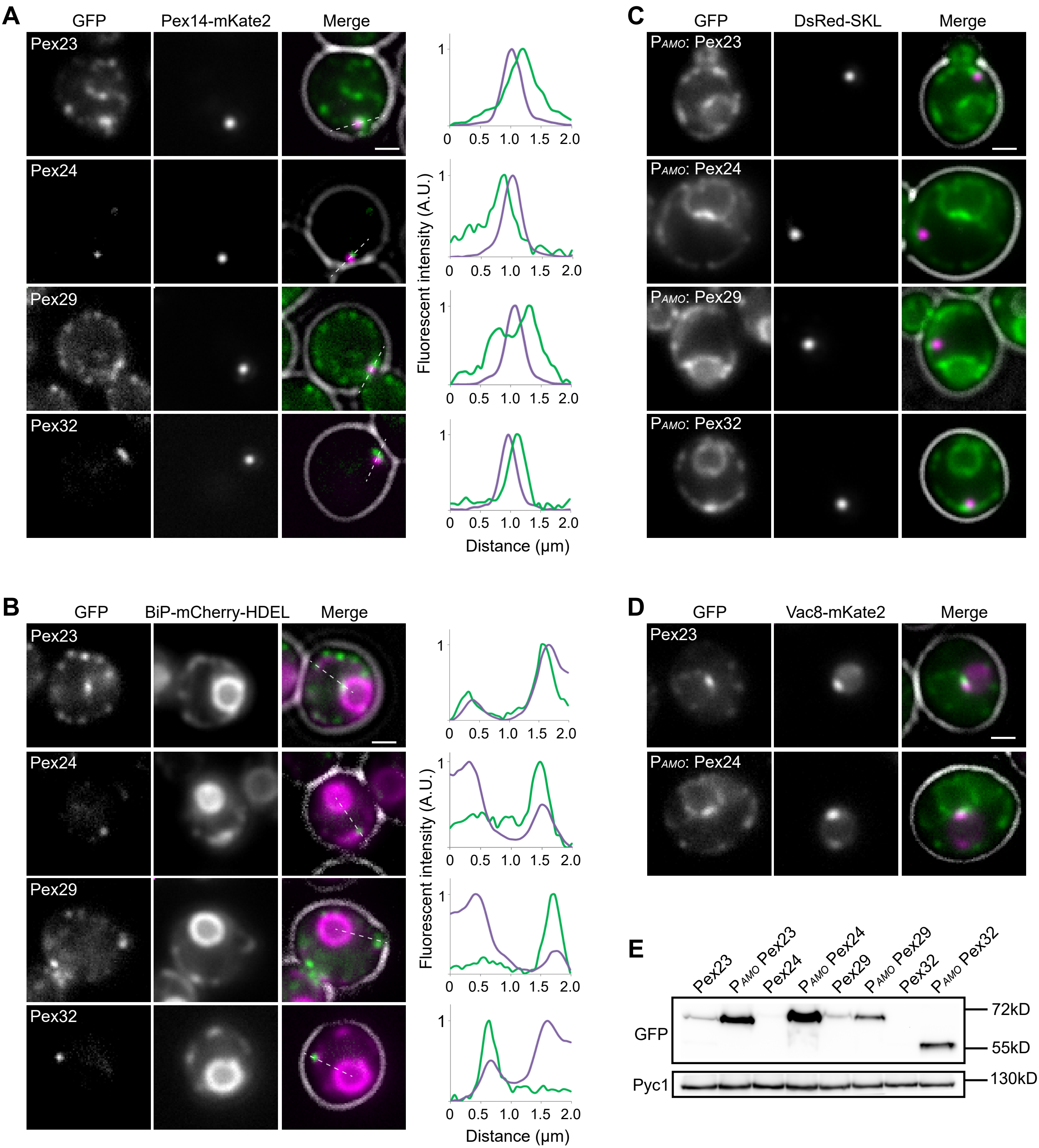
A
GFP
Pex14-mKate2
Merge
Pex23
Pex24
Pex29
Pex32
Fluorescent intensity (A.U.)
Distance (µm)
B
GFP
BiP-mCherry-HDEL
Merge
Pex23
Pex24
Pex29
Pex32
Fluorescent intensity (A.U.)
Distance (µm)
C
GFP
DsRed-SKL
Merge
PAMO: Pex23
PAMO: Pex24
PAMO: Pex29
PAMO: Pex32
D
GFP
Vac8-mKate2
Merge
Pex23
PAMO: Pex24
E
Pex23
PAMO Pex23
Pex24
PAMO Pex24
Pex29
PAMO Pex29
Pex32
PAMO Pex32
GFP
Pyc1
72kD
55kD
130kD

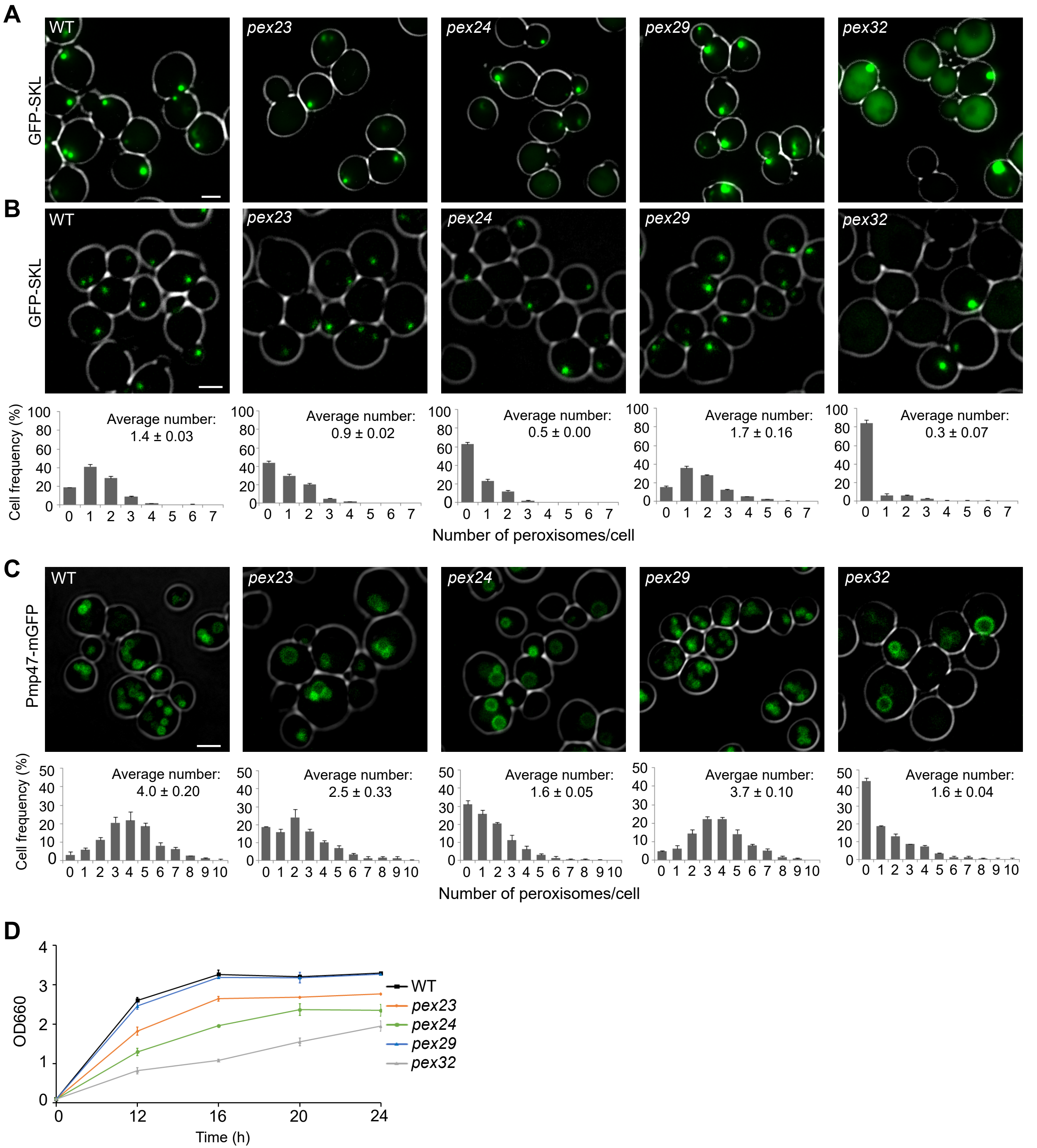
A
WT
pex23
pex24
pex29
pex32
GFP-SKL
B
WT
pex23
pex24
pex29
pex32
GFP-SKL
Cell frequency (%)
Average number:
1.4 ± 0.03
Average number:
0.9 ± 0.02
Average number:
0.5 ± 0.00
Average number:
1.7 ± 0.16
Average number:
0.3 ± 0.07
Number of peroxisomes/cell
C
WT
pex23
pex24
pex29
pex32
Pmp47-mGFP
Cell frequency (%)
Average number:
4.0 ± 0.20
Average number:
2.5 ± 0.33
Average number:
1.6 ± 0.05
Avergae number:
3.7 ± 0.10
Average number:
1.6 ± 0.04
Number of peroxisomes/cell
D
OD660
Time (h)
WT
pex23
pex24
pex29
pex32

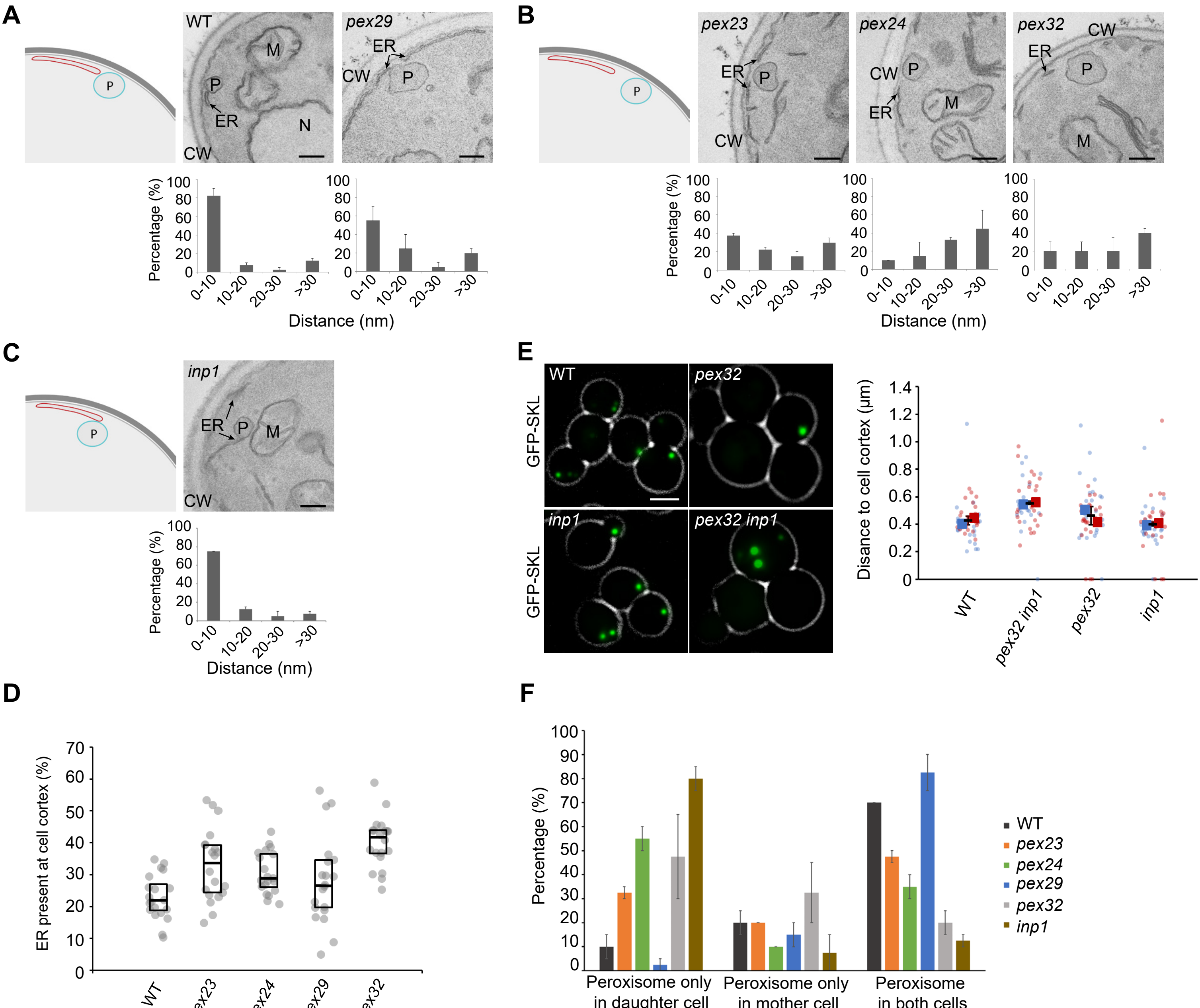
A
WT
pex29
P
M
N
ER
CW
Percentage (%)
Distance (nm)
B
pex23
pex24
pex32
C
inp1
D
ER present at cell cortex (%)
WT
pex23
pex24
pex29
pex32
E
GFP-SKL
pex32 inp1
Disance to cell cortex (µm)
F
Percentage (%)
Peroxisome only in daughter cell
Peroxisome only in mother cell
Peroxisome in both cells
0-10
10-20
20-30
>30

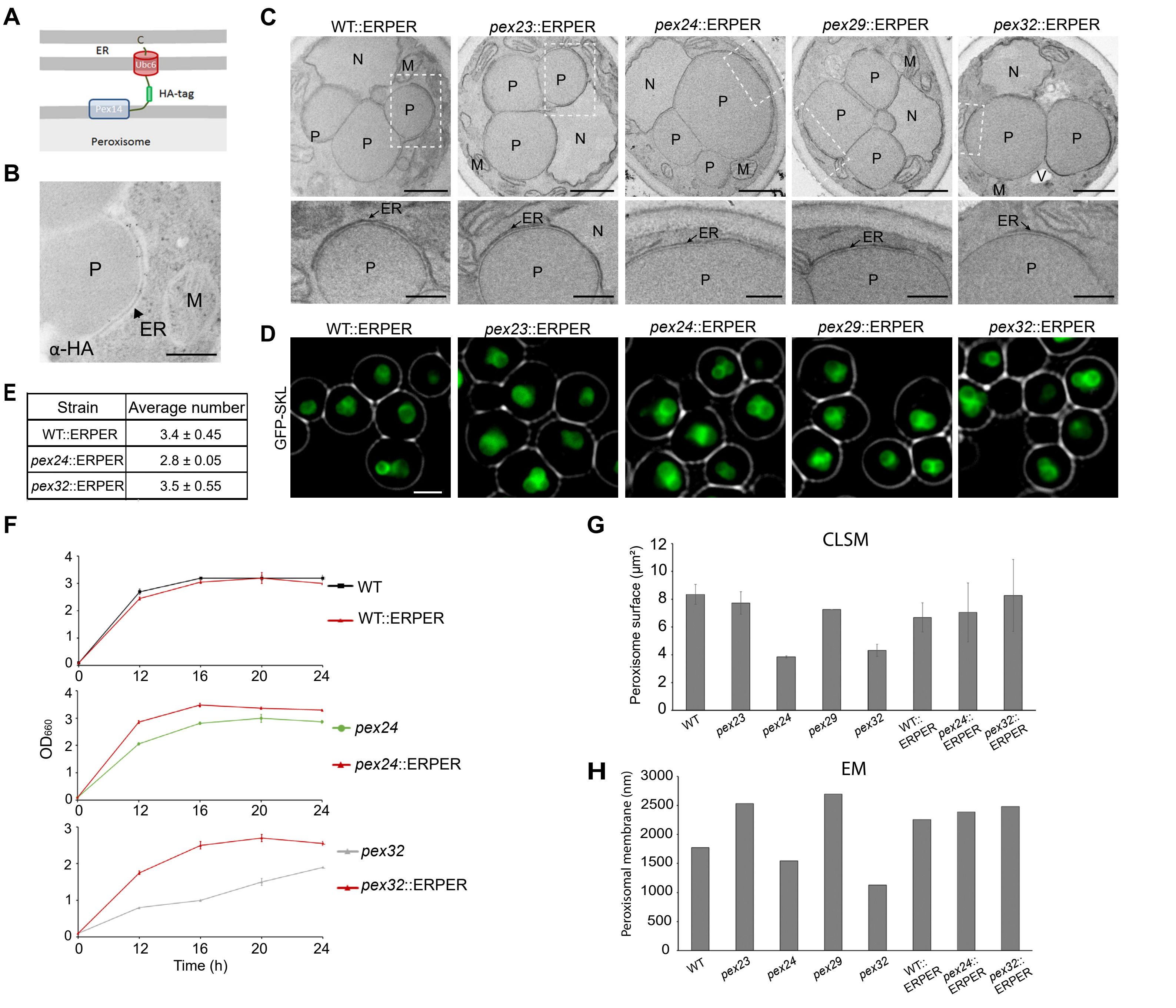

Strain	Average number
WT::ERPER	3.4 ± 0.45
pex24::ERPER	2.8 ± 0.05
pex32::ERPER	3.5 ± 0.55

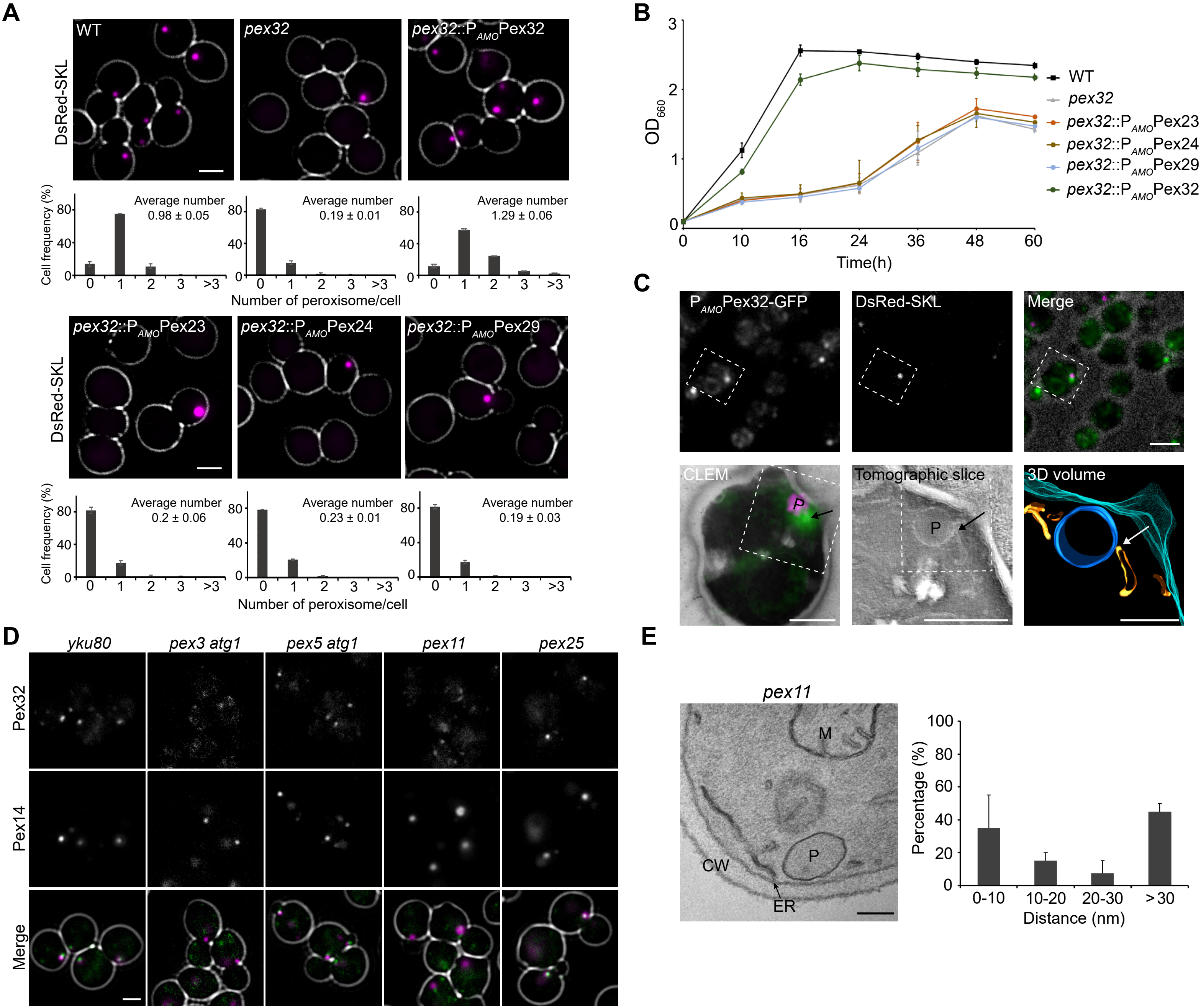

A
WT
pex32
pex32::P$_{AMO}$Pex32
DsRed-SKL
Cell frequency (%)
Average number 0.98 ± 0.05
Average number 0.19 ± 0.01
Average number 1.29 ± 0.06
Number of peroxisome/cell
pex32::P$_{AMO}$Pex23
pex32::P$_{AMO}$Pex24
pex32::P$_{AMO}$Pex29
Average number 0.2 ± 0.06
Average number 0.23 ± 0.01
Average number 0.19 ± 0.03
B
OD$_{660}$
Time(h)
WT
pex32
pex32::P$_{AMO}$Pex23
pex32::P$_{AMO}$Pex24
pex32::P$_{AMO}$Pex29
pex32::P$_{AMO}$Pex32
C
P$_{AMO}$Pex32-GFP
DsRed-SKL
Merge
CLEM
Tomographic slice
3D volume
P
D
yku80
pex3 atg1
pex5 atg1
pex11
pex25
Pex32
Pex14
Merge
E
pex11
M
P
CW
ER
Percentage (%)
Distance (nm)
0-10
10-20
20-30
>30

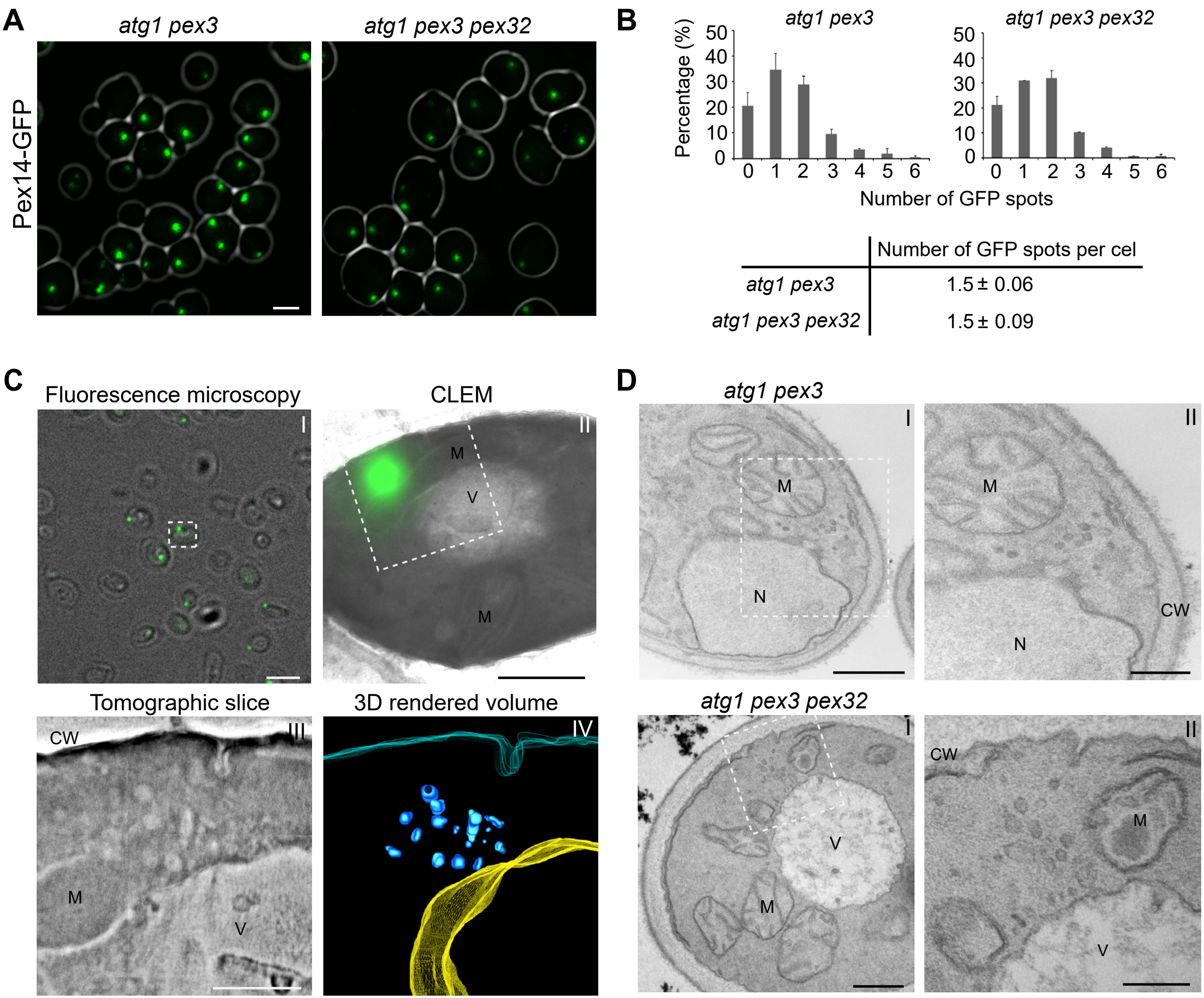
A
atg1 pex3
atg1 pex3 pex32
Pex14-GFP
B
atg1 pex3
atg1 pex3 pex32
Percentage (%)
50
40
30
20
10
0
0 1 2 3 4 5 6
Number of GFP spots
Number of GFP spots per cel
atg1 pex3 1.5 ± 0.06
atg1 pex3 pex32 1.5 ± 0.09
C
Fluorescence microscopy
I
CLEM
II
M
V
M
Tomographic slice
III
CW
M
V
3D rendered volume
IV
D
atg1 pex3
I
II
M
N
M
CW
N
atg1 pex3 pex32
I
II
V
M
CW
M
V